The Astrophysical Journal, 680:495–516, 2008 June 10

THE *SPITZER* SURVEY OF INTERSTELLAR CLOUDS IN THE GOULD BELT. I. IC 5146 OBSERVED WITH IRAC AND MIPS

Paul M. Harvey,[1] Tracy L. Huard,[2] Jes K. Jørgensen,[3] Robert A. Gutermuth,[2] Eric E. Mamajek,[2] Tyler L. Bourke,[2] Bruno Merín,[4] Lucas Cieza,[1] Tim Brooke,[5] Nicholas Chapman,[6] Juan M. Alcalá,[7] Lori E. Allen,[2] Neal J. Evans II,[1] James Di Francesco,[8] and Jason M. Kirk[9]

Received 2007 December 21; accepted 2008 February 18

ABSTRACT

We present observations of two areas totalling 0.57 deg^2 in the IC 5146 star-forming region at 3.6, 4.5, 5.8, 8.0, 24, and 70 μm observed with the *Spitzer Space Telescope*. We reexamine the issue of the distance to this cloud and conclude a value of 950 $\pm$ 80 pc is most likely. We compare source counts, colors, and magnitudes in our observed region to a subset of the SWIRE data that was processed through our pipeline. We identify more than 200 young stellar object (YSO) candidates from color-magnitude and color-color diagrams, many of which were previously unknown. We compare the colors of these YSOs to the models of Robitaille et al. and perform simple fits to the SED's to estimate properties of the circumstellar disks likely to surround the Class II and III sources. We also compare the mid-IR disk excesses to Hα emission-line data where available. We present a quantitative description of the degree of clustering, estimate the star formation efficiency, and discuss the fraction of YSOs in the region with disks relative to an estimate of the diskless YSO population. Finally, we compare the YSO distribution to the cold dust distribution mapped by SCUBA and briefly describe the diffuse emission likely due to PAHs associated with the H II region.

Subject headings: infrared: general — stars: formation

Online material: machine-readable tables

1. INTRODUCTION

The GO-4 *Spitzer* Legacy project "The Gould Belt: Star Formation in the Solar Neighborhood" (L. E. Allen et al. 2008, in preparation) is designed to complete the *Spitzer* surveys of large, nearby star-forming regions which began with the c2d Legacy Project (Evans et al. 2003). One of these newly observed clouds is IC 5146 and the dark cloud to the west of it, a region that has been extensively studied in the optical, near-IR, and millimeter molecular lines. Our *Spitzer* survey is the first large-scale mid-IR census of the young stellar objects (YSOs) in the region, as well as of the low-level diffuse dust emission.

Like the c2d project, the initial goal of these new observations is to identify the population of young stellar and substellar objects in this star-forming region, determine the relationship between these objects, their locations in the cloud relative to the cloud properties, and their evolutionary state. We report here on our observations made with *Spitzer*'s IRAC and MIPS cameras of two slightly separated portions of IC 5146, one centered on the classic "Cocoon" Nebula, the "core," that gives the region its name, and the other covering a portion of the dark cloud to the northwest, the "northwest streamer" (Fig. 1), B218. These areas were selected based on their significantly higher extinction than surrounding regions from the maps of Cambrésy (1999). Many of the condensations in the extinction map can also be identified as individual clouds in the Lynds catalog (Lynds 1962). For the remainder of this paper, when we use the identifier IC 5146, we are referring to the total region mapped in our study.

Herbig & Reipurth (2008) have recently reviewed the observational literature on the entire IC 5146 star-forming region, including studies that cover a much larger area than ours. The previous studies that are most relevant for comparison with our observations include the optical and near-IR study of Herbig & Dahm (2002) in the central region of IC 5146, and the various studies of the dust extinction and gas by Dobashi et al. (1992, 2001), Lada et al. (1994, 1999), and Kramer et al. (2003). The CO observations of Dobashi et al. (1992) and Lada et al. (1994) have shown that there are a number of molecular clumps spread over more than 2° that are probably related spatially. Lada et al. (1999) used extinction measurements to derive limits on the cloud density structure in the northern (northwest) streamer. They concluded that the streamer was roughly cylindrical with an r^{-2} density gradient. Kramer et al. (2003) correlated their submillimeter maps with the extinction maps of Lada et al. (1999) and identified high-density molecular cores where the dust emissivity appears to have increased relative to lower density regions, consistent with that expected for grain growth. In the same area of the northwest streamer, Dobashi et al. (2001) identified a number of CO outflow sources, suggesting that this was an area of very recent star formation. No published millimeter or extinction maps appear to be available for the core IC 5146 H II region, but Herbig & Dahm (2002) have published a detailed study of the stellar content of

[1] Astronomy Department, University of Texas at Austin, 1 University Station C1400, Austin, TX 78712-0259; pmh@astro.as.utexas.edu, nje@astro.as.utexas.edu, lcieza@astro.as.utexas.edu.

[2] Smithsonian Astrophysical Observatory, 60 Garden Street, Cambridge, MA 02138; leallen@cfa.harvard.edu, thuard@cfa.harvard.edu, tbourke@cfa.harvard.edu, emamajek@cfa.harvard.edu.

[3] Argelander-Institut für Astronomie, University of Bonn, Auf dem Hügel 71, 53121 Bonn, Germany; jes@astro.uni-bonn.de.

[4] Research and Scientific Support Department, ESTEC (ESA), Keplerlaan, 1, PO Box 299, 2200 AG Noordwijk, Netherlands; and Leiden Observatory, Leiden University, Postbus 9513, 2300 RA Leiden, Netherlands; bmerin@rssd.esa.int.

[5] *Spitzer* Science Center, MC 220-6, Pasadena, CA 91125; tyb@ipac.caltech.edu.

[6] Astronomy Department, University of Maryland, College Park, MD 20742; chapman@astro.umd.edu.

[7] INAF–Osservatorio Astronomico di Capodimonte, Napoli, Italy; jmae@Sun1.na.astro.it.

[8] Herzberg Institute of Astrophysics, National Research Council of Canada, Victoria, BC, Canada: james.difrancesco@nrc-cnrc.gc.ca.

[9] School of Physics and Astronomy, Cardiff University, Queens Buildings, The Parade, Cardiff CF24 3AA UK; jason.kirk@astro.cf.ac.uk.

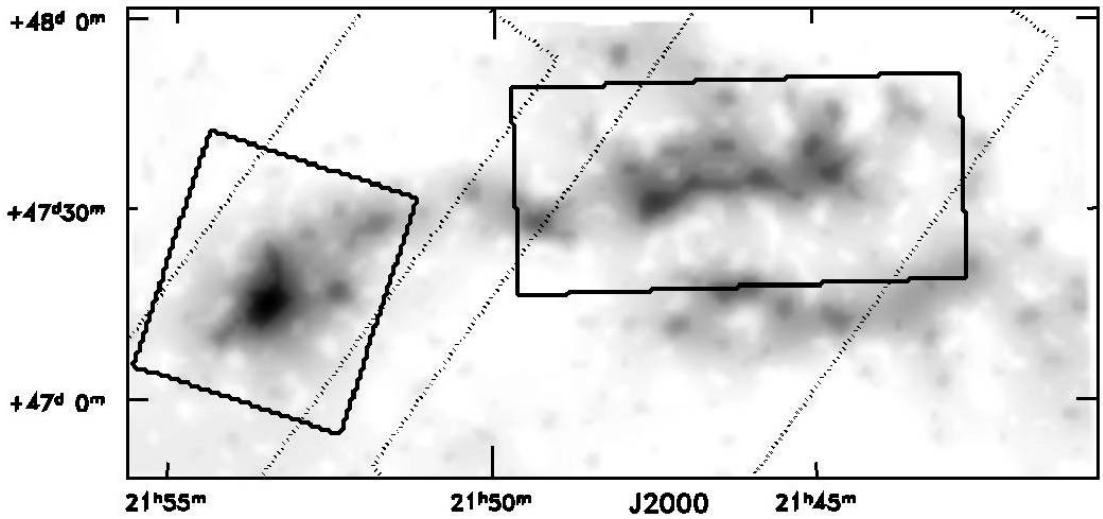

FIG. 1.—Map showing observed areas in IC 5146. The areas observed with IRAC are delineated with heavy rectangles, and those with MIPS with the lighter, dotted rectangles. These are superimposed on a grey-scale image of the extinction map of Cambrésy (1999). The "core" region comprising the optical nebula is associated with the compact area of extinction on the eastern edge of the map, while the northwest streamer is the area of higher extinction in the larger dark rectangle.

this area. They find several hundred stars that appear to lie above the main sequence and estimate a median age for the young stars of 1 Myr, although there may be a large spread in ages.

We first discuss briefly in § 2 the uncertainties in the distance to this region. In § 3 we describe the details of our observations and basic data reduction, as well as some basic statistics of the numbers of sources detected and overall issues with the data in § 3.1. In § 4 we present several color-color and color-magnitude diagrams that we use to identify the young stellar objects (YSOs) in the cloud and compare their properties with previously studied populations in c2d clouds as well as theoretical models of YSOs. In § 5 we compare our survey results to *IRAS*, some submillimeter data from SCUBA, and the optical large scale survey data and discuss several interesting individual objects. We present results of simple modeling of the circumstellar disks that are likely to surround the T Tauri–like stars in our sample and show the energy distributions of all the selected YSOs in § 6. Finally, in § 7 we estimate the total YSO population in our sampled areas and then discuss in § 8 the distribution of YSOs in the two areas studied and compare it to the distribution of gas and of dust extinction.

2. DISTANCE

Herbig & Reipurth (2008) have recently summarized the literature and previously published distance estimates for the IC 5146 cluster and its neighboring dark cloud complex. Table 1 presents all of the previously published independent distance estimates to the IC 5146 and neighboring clouds known to the authors. Distances based on the main sequence defined by the B-type stars in IC 5146 converge on ~1 kpc. The review of Herbig & Reipurth (2008) adopts the distance of 1200 ± 180 pc estimated by Herbig & Dahm (2002), which is based on the spectroscopic distances to the late-B stars using two different main-sequence calibrations. One of the distance estimates (1.1 kpc) is based on the Jaschek & Gomez (1998) absolute magnitudes for B dwarf standards with a wide range of ages. This is probably inappropriate for use with a very young population (< few Myr), and probably overestimates the absolute magnitudes assigned to the late-B stars in the young IC 5146 cluster (making IC 5146 appear more distant). The other distance (1.4 kpc) is based on the Schmidt-Kaler zero-age main sequence (ZAMS; Aller et al. 1982).

As the Schmidt-Kaler ZAMS is somewhat dated, we decided to reevaluate a photometric distance to IC 5146 using a more appropriate and modern calibrator: the Orion Nebula Cluster. The ages of the Orion and Cocoon Nebula clusters are comparable (~1 Myr), they are both still associated with nebulosity, and the ONC now has a very accurate VLBA parallax distance (414 ± 7 pc Menten et al. 2007). We dereddened *UBV* photometry from the WEBDA open cluster database for OB-type members of the ONC using the Johnson Q-method. Q is a reddening-free index defined by Johnson & Morgan (1953) as $(U - B) - 0.72(B - V)$. From a fit of $U - B$ versus $B - V$ for nearby unreddened B-type stars within 75 pc from *Hipparcos*

TABLE 1
DISTANCES TO IC 5146 AND CLOUD

Reference	Distance (pc)	Target	Notes
Walker (1959)	1000	IC 5146 cluster	Johnson & Hiltner (1956) ZAMS
Crampton & Fisher (1974)	960	BD +46 3474	Walborn (1972) ZAMS
Elias (1978)	900 ± 100	IC 5146 cluster	Blaauw (1963) ZAMS
Forte & Orsatti (1984)	1000	IC 5146 cluster	Balona & Feast (1975) ZAMS
Lada et al. (1999)	460^{+40}_{-60}	North cloud	Star counts
Herbig & Dahm (2002)	1400 ± 180	IC 5146 cluster	Aller et al. (1982) ZAMS
Herbig & Dahm (2002)	1100 ± 180	IC 5146 cluster	Jaschek & Gomez (1998) MS
This work	950 ± 80	IC 5146 cluster	ONC ZAMS

(using UBV photometry from J. C. Mermilliod[10]), we find that $(B-V)_0 = 0.294Q - 0.023$ (this line also nicely fits the blue envelope of all OB stars in the *Hipparcos* catalog with UBV photometry in Mermilliod). As both the IC 5146 and ONC members contained unresolved binaries, we do not attempt to fit a single-star ZAMS, but simply fit a quadratic to all of the unevolved ONC OB-stars (ignoring the O9 III star ι Ori) and find for ONC: $M_v = 1.556 + 9.842(B-V)_0 - 24.73(B-V)_0^2$, with rms = 0.48 mag ($-0.3 < (B-V)_0 < -0.02$).

For the *B*-type members of IC 5146, we adopt the UBV photometry of Herbig & Dahm (2002) and use the *Q*-method to estimate the intrinsic $B-V$ colors. The reddening law for stars in the core H II region in IC 5146 is consistent with the normal interstellar reddening law as discussed by both Walker (1959) and Forte & Orsatti (1984). In addition, our analysis also points to a normal reddening law in this region since the dereddened $B-V$ colors from the *Q*-method agree reasonably well with those expected for stars with measured spectral types. Using the ONC absolute magnitude calibration, we find that the two famous members (BD +46 3474 [B1 V] and 3471 [B9.5e]) give low distances ~350–400 pc, while the rest of the late-B types stars (Walker nos. 35, 53, 62, 64, and 76) give distance moduli consistent with $(m-M)_0 = 9.89$ mag (standard error 0.18 mag, standard deviation 0.40 mag). Given that the rms in the fit to the ONC members is 0.48 mag, the IC 5146 late-B stars appear to be consistent with being a codistant main sequence (including unresolved binaries). We discount the "near" distance of ~350–400 pc on the following grounds. Herbig & Dahm (2002) note that their low-mass pre-MS stars are consistent with having a mean age of 200 kyr at a distance of 1200 pc on the evolutionary tracks of D'Antona & Mazzitelli (1997) (see Fig. 7 of Herbig & Dahm 2002). If one moves the cluster to ~375 pc, the ages of the K/M-type T Tauri stars jump from ~0.2 to ~15 Myr. We can exclude this isochronal age based on the appearance of the nebulosity associated with IC 5146 and the high number of accreting pre-MS stars. Both factors argue for an age of <few Myr. Also *all* of the late-B type candidate members would have to be nonmembers, as their color-magnitude position at $d \simeq 400$ pc would put them ~2 mag below the main sequence. On these grounds, we can also discount the "near" distance advocated by Lada et al. (1999) of 460 pc.

It is not surprising that BD +46 3471 and 3474 give discrepant distance moduli. As the most massive member, BD +46 3474 might be somewhat evolved, so its ZAMS distance (400 pc) is suspect. BD +46 3471 is a Herbig Be star and may be overluminous due to being pre-MS (its ZAMS distance is 355 pc). Given the self-consistency of the distance moduli to the other late-B stars, we reject the short distances to BD +46 3471 and 3474, and adopt $(m-M)_0 = 9.89 \pm 0.18$ mag or $D = 950 \pm 80$ pc. This agrees well with the previous estimates of Walker (1959), Crampton & Fisher (1974), Elias (1978), and Forte & Orsatti (1984). Moving the pre-MS population from Herbig & Dahm's 1200 pc to 950 pc forces the lower mass pre-MS population to be somewhat older, ~0.6 Myr, than their estimate of 0.2 Myr.

2.1. *Argument for Codistance of IC 5146 and B218 Cloud*

The shortest distance (460 pc) is derived from a star-count analysis of the "northern streamer" by Lada et al. (1999). The technique counts the number of low-extinction stars within the $A_V = 10$ contours of the cloud, and employs a Wainscoat et al. (1992) model to predict the number of low-extinction stars that should be seen as a function of distance. We discount the possibility that the IC 5146 cluster itself could be at 460 pc, as this would place its B-star population well below the ZAMS. Given the general agreement among the distance estimates to the IC 5146 clusters (~1 kpc), we are in a position to believe that either (1) the Lada et al. (1999) distance is correct, and the northern streamer is not codistant with the IC 5146 cluster, or (2) the Lada et al. (1999) distance is incorrect, and the Northern Streamer and IC 5146 cluster are codistant.

There is good circumstantial evidence supporting the notion that the Northern Streamer and IC 5146 cluster are approximately codistant. First, the young stellar cluster in IC 5146 is clearly interacting with the dense molecular gas in its vicinity producing the Cocoon Nebula H II region (IC 5146 = Sharpless 125). Geometrically, the molecular gas associated with the IC 5146 cluster appears to be at the end of a long (~2°) filament (Barnard 168), extending from L1010 as first noted by Barnard (1919). The molecular gas in the Barnard 168 complex ("IC 5146 dark cloud") shows a velocity gradient, and the molecular gas associated with IC 5146 has velocities consistent with the gradient seen in the rest of the dark cloud (Dobashi et al. 1992). Velocity-integrated CO maps of the region (Dobashi et al. 1992) and extinction maps (Dobashi et al. 2005) show that IC 5146 and the B 218 clouds are well separated from other dark cloud complexes in this region. Given the circumstantial evidence, it is unlikely that IC 5146 and B 218 (IC 5146 dark cloud, including Northern Streamer) are at very different distances.

3. OBSERVATIONS AND DATA REDUCTION

The areas chosen for mapping are shown graphically in Figure 1. Both areas were observed twice with *Spitzer*'s IRAC and MIPS cameras with the AORs and dates shown in Table 2. The ecliptic latitude of this area, ~+55°, is high enough that asteroids will be essentially nonexistent, although our two-epoch mapping strategy would eliminate any that were present.

The most important parts of the data processing start with a check of the images, some image corrections for obvious problems, and creation of mask files noting pixels that may be problematic. Following this the individual frames are mosaicked, both the individual epochs separately and the entire data set. Sources are located in the mosaics and then reextracted from the stack of individual images that include each source position. Finally, the source lists for each wavelength are band-merged, and sources that are not detected at some wavelength(s) are "band-filled" to find approximate fluxes or upper limits at the positions derived at wavelengths where the source was reliably extracted.

The details of this data reduction are essentially identical to those used for all the c2d data with the exception of the state of the *Spitzer* BCD pipeline used as input to the c2d pipeline (Table 2). The c2d pipeline processing of IRAC data has been described by Harvey et al. (2006) for MIPS by Young (2005) and Rebull et al. (2007). In addition, Harvey et al. (2007) describe a number of other reduction processes that were also used for these data on IC 5146. A detailed description of all this processing is included in the documentation for the final delivery of c2d data to the SSC.[11]

[10] See J. C. Mermilliod 1991, Catalogue of Homogeneous Means in the UBV System, Institut d'Astronomie, Universite de Lausanne, VizieR Online Catalog, II/168.

[11] See N. J. Evans II et al. (2007), at http://irsa.ipac.caltech.edu/data/SPITZER/C2D/doc.

TABLE 2

OBSERVATIONS SUMMARY

AOR	Date	Program ID	BCD Version	Region	Area (deg^2)
		IRAC Observations			
0003651072.....	2004 Jun 10	IRAC GTO/6	S14	Core	
0019991040.....	2006 Nov 26	30574	S15	Core	0.29[a]
0019978752.....	2006 Nov 26	30574	S15	Northwest	
0020003584.....	2006 Nov 26	30574	S15	Northwest	0.47[a]
		MIPS Observations			
0019982448.....	2007 Jan 6	30574	S15	Core	
0019982592.....	2007 Jan 9	30574	S15	Core	0.83[a]
0020016128.....	2007 Jan 6	30574	S15	Northwest	
0020015616.....	2007 Jan 9	30574	S15	Northwest	1.46[a]

[a] The combined area for both epochs in this region.

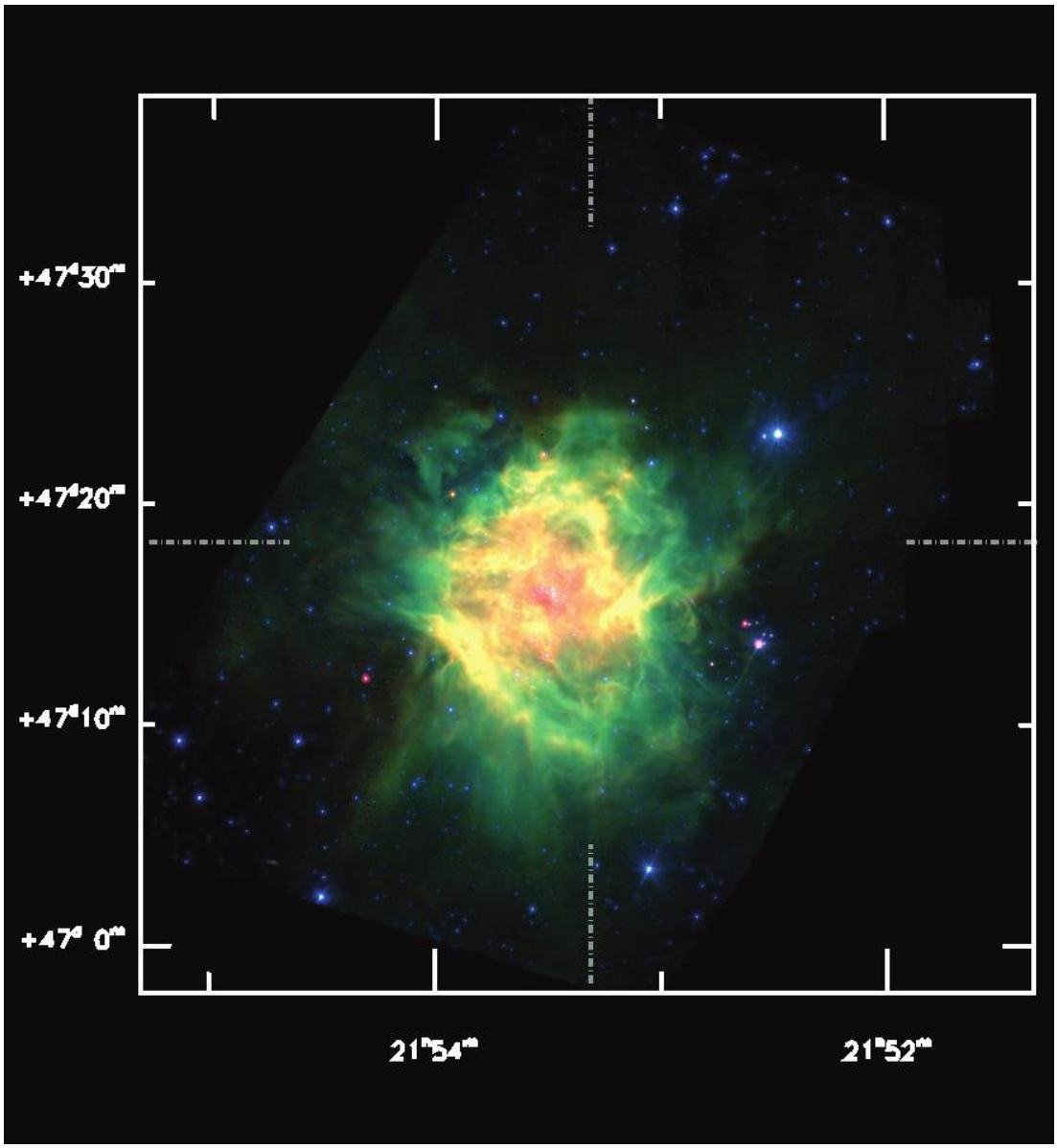

FIG. 2.—Color image made from IRAC2 (*blue*), IRAC4 (*green*), and MIPS1 (*red*) images, for the area observed in common of the central region of IC 5146. Note that this area is considerably smaller than either of the areas observed with one instrument only. The dash-dot lines indicate where the spatial cuts in Fig. 24 were made.

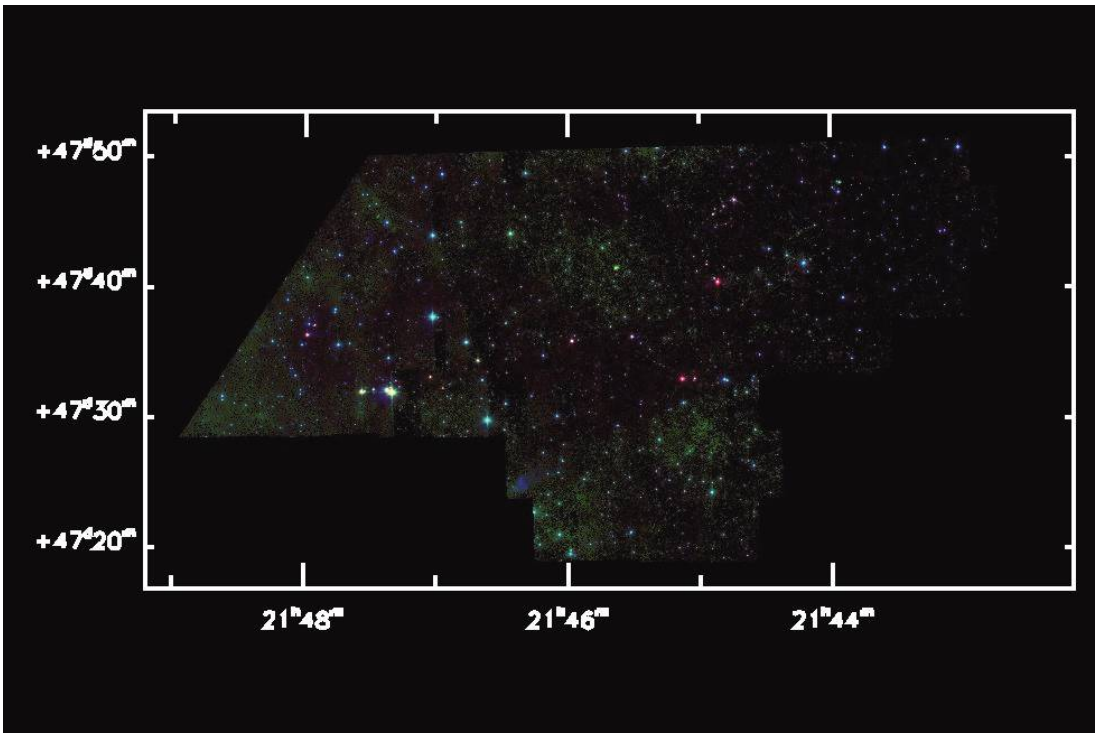

FIG. 3.—Color image made from IRAC2 (*blue*), IRAC4 (i), and MIPS1 (*red*) images, for the area observed in common of the "northwest streamer."

Figures 2 and 3 show color mosaics using IRAC bands 2 and 4 and MIPS 24 μm of the entire mapped areas that have IRAC and MIPS data. We also discuss the diffuse emission in Figure 2 in § 8.2.

3.1. *Source Statistics*

Table 3 lists the total number of sources extracted in each band for the entire observed region in both IC 5146 and the northwest streamer at S/N $> 5\ \sigma$, along with several subsets of the total. As was the case for the star-forming regions observed in the c2d program, most of the objects detected in our survey are background/foreground stars at the brighter flux levels. At fluxes within a factor of 10 of our detection limits, extragalactic objects make a substantial contribution to the source counts as well. As we discuss in the following sections, the total number of YSOs identified in our study in the observed area is of order 200.

TABLE 3
IC 5146 DETECTION STATISTICS

Wavelength(s)	Number of Sources
3.6 μm $> 5\ \sigma$	76038
4.5 μm $> 5\ \sigma$	57551
5.8 μm $> 5\ \sigma$	11650
8.0 μm $> 5\ \sigma$	7128
All four IRAC bands $> 5\ \sigma$	4749
Any IRAC band and 2MASS $K_s > 5\ \sigma$	24273
24 μm $> 5\ \sigma$	1305
70 μm $> 5\ \sigma$	11
24 and 70 μm $> 5\ \sigma$	10
24 μm and 2MASS $K_s > 5\ \sigma$	728
24 μm and any IRAC	631[a]
70 μm and any IRAC	7

[a] The greater number of matches between 24 μm and K_s vs. IRAC is due to the smaller area coverage of the IRAC data.

4. YSO SELECTION

A number of authors have discussed criteria for identifying YSOs from *Spitzer* data combined with shorter and/or longer wavelength data. These criteria are typically based on some combination of infrared excess together with a brightness limit, below which extragalactic contamination becomes too significant to be able to reliably separate such objects. Harvey et al. (2006) discussed a relatively simple color and magnitude criterion based on IRAC colors. Rebull et al. (2007) formulated a similar criterion based on the combination of MIPS 24 μm and 2MASS K_s magnitudes. For sources with both IRAC and MIPS observations, Harvey et al. (2007) described a multifaceted set of selection criteria using several combinations of *Spitzer* and 2MASS data to

TABLE 4
YSO SELECTION CRITERIA WHEN FIVE-BAND DATA NOT AVAILABLE

Criterion	Value for YSOs
MIPS/2MASS Criteria	
24 μm S/N	>5
2.2 μm S/N	>5
K_s	<14
[24]	<10
k_s − [24]	>2
IRAC-Only Criteria	
[4.5]	<13
[4.5] − [8.0]	>1
Not bandfilled at 8 μm	True

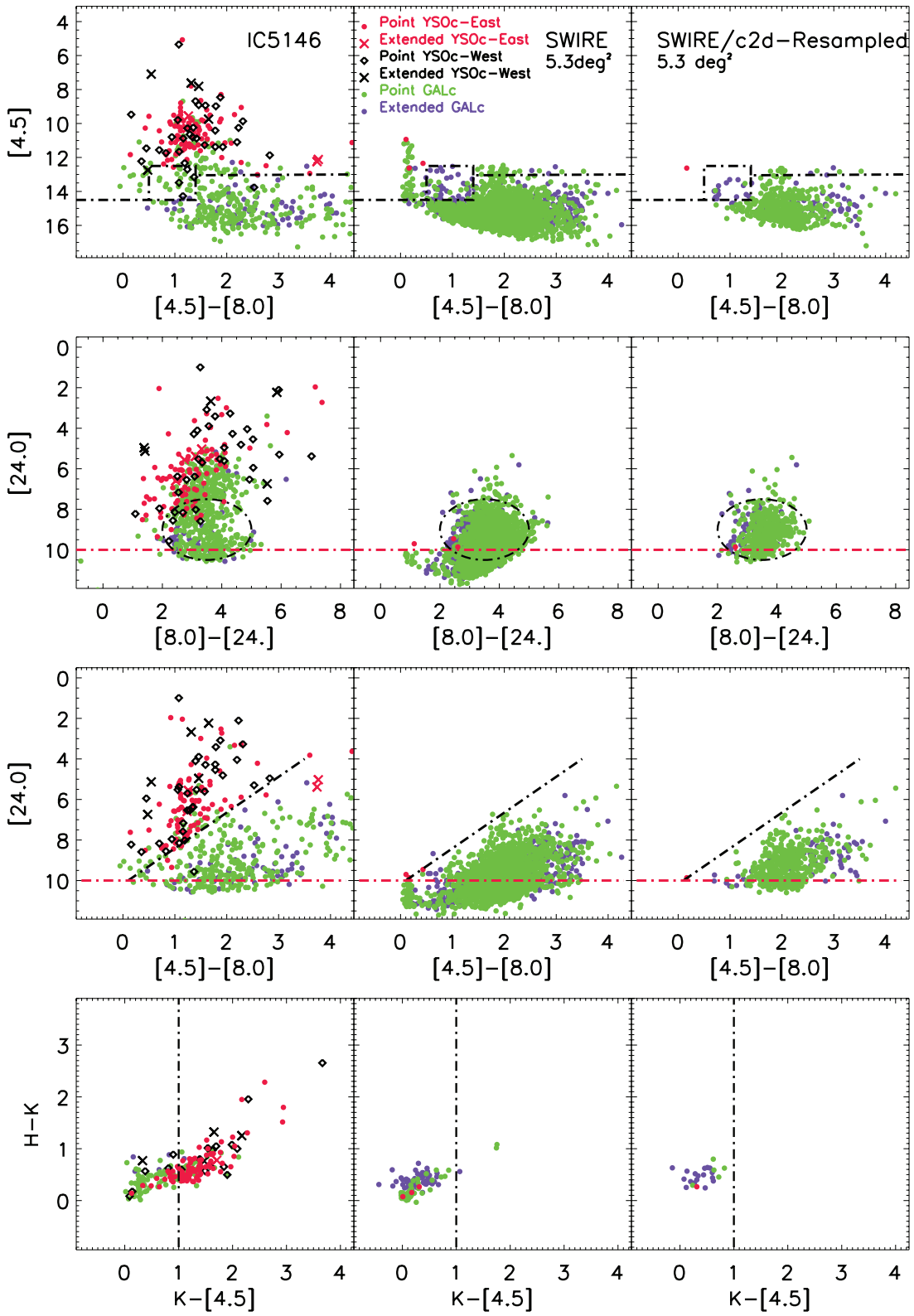

FIG. 4.—Color-magnitude and color-color diagrams for IC 5146 (*left*), full SWIRE (*center*), and trimmed SWIRE regions. The black dot-dashed lines show the "fuzzy" color-magnitude cuts that define the YSO candidate criterion in the various color-magnitude spaces. The red dot-dashed lines show hard limits, fainter than which objects are excluded from the YSO category.

TABLE 5
YSO Candidates in IC 5146 Based on IRAC and MIPS

ID	Name/Position (SSTgbsJ)	Previous Name (Simbad)	3.6 μm (mJy)	4.5 μm (mJy)	5.8 μm (mJy)	8.0 μm (mJy)	24.0 μm (mJy)	70.0 μm (mJy)
1.....	21435613+4748083	TYC 3595-1670-1	14.6 ± 0.7	9.92 ± 0.47	7.36 ± 0.35	11.6 ± 0.8	17.3 ± 1.6	...
2.....	21444308+4746436	IRAS 21428+4732	0.29 ± 0.02	1.43 ± 0.09	1.88 ± 0.12	0.79 ± 0.06	14.4 ± 1.4	...
3.....	21444447+4746498	IRAS 21428+4732	44.8 ± 2.2	49.0 ± 2.4	50.7 ± 2.4	67.1 ± 3.2	199 ± 18	...
4.....	21444831+4744597		0.15 ± 0.01	0.56 ± 0.03	1.18 ± 0.07	2.06 ± 0.10	54.4 ± 5.1	...
5.....	21444918+4746212		22.6 ± 1.1	21.8 ± 1.0	19.8 ± 0.9	20.6 ± 1.0	44.3 ± 4.1	...

Note.—Table 5 is published in its entirety in the electronic edition of the *Astrophysical Journal*. A portion is shown here for guidance regarding its form and content.

provide a relatively high confidence set of YSOs in the Serpens Cloud. The latter set of criteria have been applied by Alcala et al. (2008) in Cha II and by Merín et al. (2008) in Lupus, and the vast majority of the *Spitzer*-selected YSOs have been confirmed spectroscopically. Because our observations of IC 5146 have substantial areas with only IRAC or only MIPS data, in addition to the overlap areas, we make use of all these previous suggestions for YSO identification.

For the cases where we have MIPS 24 μm data, we have used criteria identical to those of Rebull et al. (2007) when four-band IRAC data are not available, and those of Harvey et al. (2007) when the IRAC data are available. The situation with respect to IRAC-only areas, however, is slightly more complex. In addition to the areas with no observations at 24 μm, there are significant areas in the core of IC 5146 that have very bright diffuse 8 and 24 μm emission (Fig. 2), presumably emission from small dust grains heated by early type stars within the nebula (see discussion in § 8.2). In these areas, the detection limits at 24 μm and sometimes at 8 μm are poor enough that the $[8.0] - [24.0]$ color is impossible to determine reliably. Therefore, it is impossible to use the selection criterion based on $[8.0] - [24.0]$ color versus [24] used in other regions with five-band coverage. For possible YSOs in these areas, we have used the same criteria as in the IRAC-only areas, but with an additional constraint that we do not include as candidates those sources that have been "band-filled" at both 8 and 24 μm (i.e., not in the original extraction list at those wavelengths). Table 4 summarizes the main parts of the selection criteria for the IRAC-only and MIPS-only selected YSOs. We note that these criteria were all chosen to *eliminate* contaminating sources, e.g., stellar photospheres and extragalactic objects, not to *identify* YSOs. Therefore, as we discuss below, they do not depend on the distance to the particular star-forming region being observed.

Figure 4 shows graphically the most important criteria for sources with both IRAC and MIPS data, using exactly the same limits as did Harvey et al. (2007). In addition to the color-magnitude and color-diagrams for the IC 5146 YSOs, we also show the same diagrams for two versions of a sample of the Elais N1 data set in the SWIRE extragalactic survey (Surace et al. 2004). The central column of panels shows the full sample of sources in a 5.3 deg^2 area while the right panel shows a "trimmed" sample with the sensitivity limits of our survey imposed on the same sources and a level of extinction applied comparable to that derived from our extinction maps. These processes have been described in detail by Harvey et al. (2007). These comparisons show the extent to which our combined IRAC/MIPS selection criteria are effective in eliminating most extragalactic contaminants. Tables 5, 6, and 7 list the YSOs that match these criteria. Tables 6 and 7 are specifically labeled as "candidates" because of the lesser reliability of our selection process without a full *Spitzer* data set. Finally, as did Harvey et al. (2007), after careful examination of the images and/or photometry, we have eliminated some objects from these tables that did fit the nominal criteria. These typically included objects that appeared to be possibly extended like galaxies or objects whose photometry might be suspect due to contamination by a nearby source or partial saturation.

It is important to note that the YSO selection criteria were all developed using data from clouds much closer than IC 5146. Therefore, the typical cutoff between YSOs and contaminating background extragalactic sources occurs at a much higher luminosity level for the YSOs in IC 5146 than it did for the c2d clouds where the criteria were developed. Figure 4 shows, however, that since the criteria for elimination of extragalactic contaminants are based solely on the observables, color and magnitude, that effect of simply limiting our YSO selection to higher luminosity objects is probably the only effect of applying the c2d criteria to IC 5146.

The final sample of 202 YSO candidates given in Tables 5, 6, and 7 is comprised largely of objects that fall into the "Class II" category based on the spectral energy distributions (SEDs; Greene et al. 1994).

Table 8 lists the number of sources in each of the separate areas that fall nominally into Greene's four categories of SEDs, I ($\alpha \geq 0.3$), flat ($-0.3 \geq \alpha < 0.3$), II ($-1.6 \geq \alpha < -0.3$), and III ($\alpha < -1.6$), that are an extension of the original class system described by Lada (1987). The spectral slopes α are calculated

TABLE 6
YSO Candidates in IC 5146 Based on MIPS/2MASS

ID	Name/Position (SSTgbsJ...)	Previous Name (Simbad)	3.6 μm (mJy)	4.5 μm (mJy)	5.8 μm (mJy)	8.0 μm (mJy)	24.0 μm (mJy)	70.0 μm (mJy)
133.....	21423517+4740150		...	...	...	...	43.4 ± 4.0	...
134.....	21434976+4724450		...	...	...	...	12.8 ± 1.2	...
135.....	21441820+4723438		...	...	...	...	11.1 ± 1.0	...
136.....	21442231+4716427		...	...	...	...	3.27 ± 0.34	...
137.....	21442631+4718113		14.8 ± 0.7	...	24.0 ± 1.2	...	108 ± 10	...

Note.—Table 6 is published in its entirety in the electronic edition of the *Astrophysical Journal*. A portion is shown here for guidance regarding its form and content.

TABLE 7
YSO Candidates in IC 5146 Based on IRAC Only

ID	Name/Position (SSTgbsJ...)	Previoius Name (Simbad)	3.6 μm (mJy)	4.5 μm (mJy)	5.8 μm (mJy)	8.0 μm (mJy)	24.0 μm (mJy)	70.0 μm (mJy)
176.....	21472922+4732166		2.89 ± 0.14	5.67 ± 0.27	7.38 ± 0.36	7.67 ± 0.37	< 5.30	...
177.....	21485261+4731309		61.1 ± 3.0	60.2 ± 2.9	57.4 ± 2.7	62.1 ± 3.0	...	...
178.....	21485607+4730291		0.42 ± 0.03	2.18 ± 0.12	4.27 ± 0.21	5.42 ± 0.26	...	...
179.....	21491143+4728422		4.71 ± 0.22	5.10 ± 0.26	5.56 ± 0.26	8.33 ± 0.41	...	...
180.....	21491245+4730189		20.6 ± 1.0	24.5 ± 1.2	26.1 ± 1.2	30.0 ± 1.4	...	...

Note.—Table 7 is published in its entirety in the electronic edition of the *Astrophysical Journal*. A portion is shown here for guidance regarding its form and content.

over the widest range possible where data were available between 2.2 and 24 μm. Figure 5 shows a histogram of the distribution of spectral slopes, α, for each of the two mapped areas. It is clear from both Table 8 and Figure 5 that the northwest streamer region has a much higher fraction of SED's characteristic of less-evolved objects (Class I and flat) than does the core region containing the nebula that defines IC 5146.

Robitaille et al. (2006) have computed a grid of 200,000 models of YSOs covering a wide range in luminosity, circumstellar mass density, and inclination. For comparison with our similar plots for Serpens (Harvey et al. 2007), we show here (Fig. 6) the same color-color and color-magnitude distributions for the YSOs in IC 5146 compared to a model cluster from Robitaille et al. (2006) assuming a distance of 950 pc. We see here the same effect noted in the previous paragraph that the northwest streamer contains a higher fraction of less evolved objects than does the core of IC 5146. Figure 6 also shows that there is no significant difference in the distribution of YSO colors for two different luminosity groups, above or below 1 $L_{\odot}$. This is consistent with the findings of Harvey et al. (2007) for Serpens, although we have not been able to probe to nearly as low luminosities in this study of IC 5146 because of its greater distance. The similarity of colors for fainter and brighter YSOs is consistent also with our conclusion that we have eliminated most extragalactic contaminants with our selection criteria.

5. COMPARISON WITH *IRAS*, OPTICAL, AND SUBMILLIMETER DATA

There are nine *IRAS* sources detected at 12 μm that are located within the area of the IC 5146 core that we have mapped with either IRAC or MIPS. Of these, three appear to be clearly detected as point sources by *Spitzer*, and the other six are within the bright, diffuse nebulosity seen at all *Spitzer* wavelengths. These latter six probably represent the response of the *IRAS* detectors to gradients in the nebulosity. In contrast, all seven *IRAS* 12 μm sources in the northwest streamer have clear pointlike *Spitzer* sources associated with them.

Table 9 lists the optical sources catalogued by Herbig & Dahm (2002) near the core of IC 5146 and the best-matching *Spitzer* sources within 4″ of the optical position. The vast majority of the optical sources appear to have bona fide *Spitzer* sources associated with them. Herbig & Dahm observed a subset of their sources spectroscopically to search for Hα emission. Figure 7 displays the IR excess properties of the sources with Hα measurements in terms of the Hα equivalent width versus the [3.6] − [8.0] color of the best-matching *Spitzer* source. This figure shows that most of the optical sources with Hα equivalent widths above 10 Å have obvious IR excess emission as indicated by spectral slopes α greater than −2. Likewise the majority of the sources with Hα equivalent widths below 5 Å have little or no IR excess emission. There are, however, exceptions to both these trends. The two objects in the lower right part of the diagram with nearly photospheric spectral slopes but larger Hα fluxes are numbers 595 and 677 in Table 9, while the single object with small Hα flux but strong IR excess is number 622. There is little or no quantitative correlation beyond this general relationship between the IR spectral slope and the Hα equivalent width. These results are similar to those found in other studies of IR excess correlations with Hα emission (Haisch et al. 2001; Martin 1997), and agree within the mutual spread of the distributions with the results of Lada et al. (2006) shown in their Figure 9. At some level this correlation suggests a roughly coeval evolution of the gas and dust components of the circumstellar disks. Littlefair et al. (2004)

TABLE 8
Number of Sources vs. Spectral Slope (α)

α Category	Eastern Core	Northwest Streamer
I.....	13	16
Flat	9	3
II.....	69	18
III.....	2	2

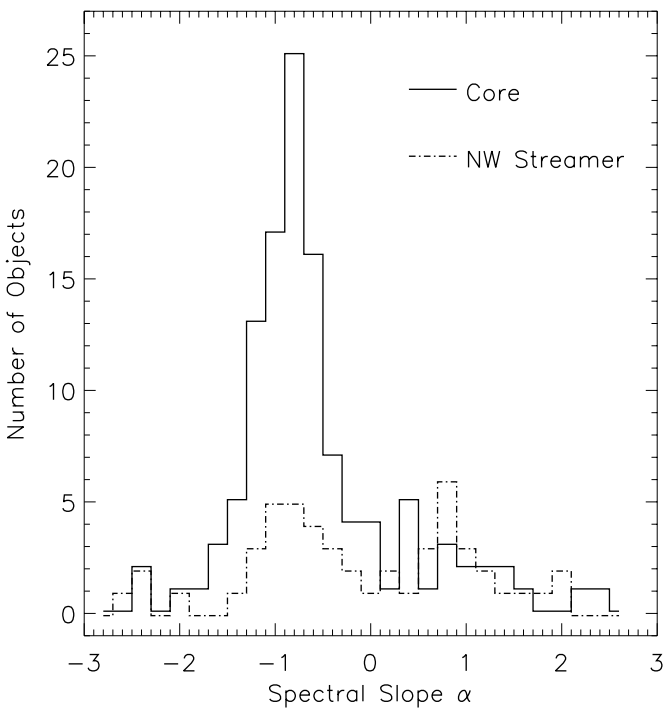

Fig. 5.—Histogram of distribution of spectral slopes, "alpha," for the 132 YSOs selected by the combined IRAC and MIPS data in IC 5146.

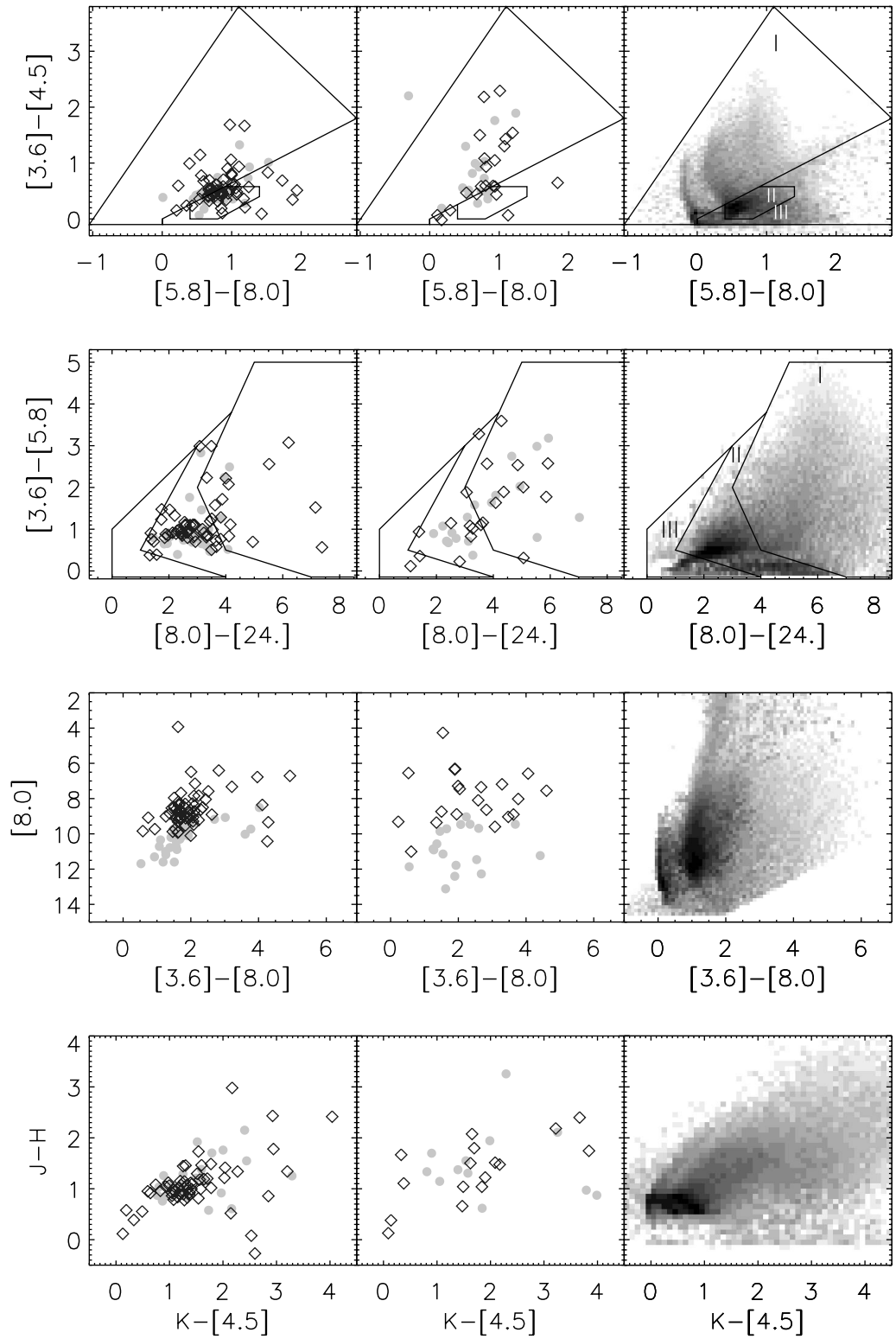

FIG. 6.—Color-color and color-magnitude plots of the YSOs in the "core" of IC 5146 (*left panels*), the northwest streamer (*center panels*), and the density distribution of models from Robitaille et al. (2006). The YSOs plotted are the 93 IC 5146 five-band YSOs in the core region and the 39 five-band YSOs in the northwest streamer. The symbols are for the two different luminosity groups discussed in the text: open diamonds for $L > 1\,L_{\odot}$, and light filled circles for $0.02\,L_{\odot} < L < 1\,L_{\odot}$. The model data were those for their model cluster, with a distance of 950 pc for IC 5146 and with our observed completeness limits. Also shown are the rough areas occupied by mainly stage I, II, and III models from Robitaille et al. (2006).

TABLE 9
Spitzer Matches to Herbig and Dahm Optical Sources

Optical Number	Offset (arcsec)	*Spitzer* Match (SSTgbsJ...)	YSO Number (Tables 5–7)	3.6 μm (mJy)	4.5 μm (mJy)	5.8 μm (mJy)	8.0 μm (mJy)	24.0 μm (mJy)
1.....	0.6	21530456+4712549		2.05 ± 0.14	1.25 ± 0.07	0.84 ± 0.30	<3.06	<4.78
2.....	0.7	21530479+4716582		1.09 ± 0.08	0.68 ± 0.05	0.84 ± 0.34	<7.70	<17.9
3.....	0.6	21530502+4712125		36.5 ± 2.0	21.7 ± 1.1	16.8 ± 0.9	10.4 ± 0.8	1.91 ± 0.86
4.....	0.4	21530524+4716152		2.22 ± 0.12	1.41 ± 0.08	0.83 ± 0.29	<2.94	<15.2
5.....	1.1	21530520+4715524		0.60 ± 0.06	0.37 ± 0.03	<2.27	<5.90	<13.7

Note.—Table 8 is published in its entirety in the electronic edition of the *Astrophysical Journal*. A portion is shown here for guidance regarding its form and content.

have suggested that some WTTs with weak Hα emission may actually be in such a high state of accretion that the accreting material is optically thick. This could certainly explain some of the scatter in Figure 7, although flare activity is another possibility also.

5.1. *Selected Sources*

We describe here some details of sources discussed individually by Herbig & Reipurth (2008).

BD +46 3474.—Our *Spitzer* images of this object, the exciting star for IC 5146, are overlaid with very bright, diffuse nebulosity as shown in Figure 2. In spite of this, it is still possible to identify the character of the object at the center. The source is definitely elongated and nonstellar in appearance in the IRAC and MIPS 24 μm bands (see Fig. 8). The IRAC colors of this object are consistent with essentially no excess emission above the photosphere, and so it was classified as a "star" in our initial search for IR-excess objects. There is a low S/N detection of a 24 μm excess, but the bright nebulosity pervading this area makes that measurement quite unreliable.

BD +46 3471.—As described by Herbig & Reipurth (2008), this is a classic HAeBe star in the area and has several fainter IR-excess objects nearby. This is YSO 47 in Table 5. Despite its 24 μm flux density in excess of 1000 mJy, there is no obvious source in our 70 μm map.

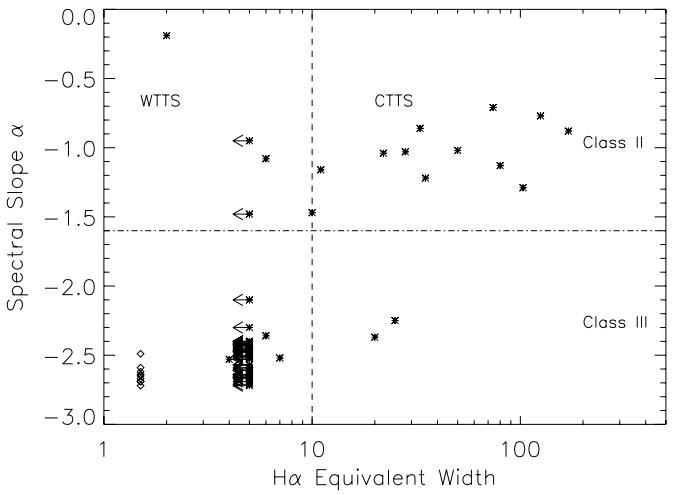

Fig. 7.—Plot of Hα flux vs. IR excess as measured by the [3.6] − [8.0] *Spitzer* colors for sources in common with those observed by Herbig & Dahm (2002). The nominal dividing line in Hα strength between WTTS and Classical TTS is shown (*dashed line*) at 10 Å equivalent width, and the nominal dividing line in spectral slope at $\alpha = -1.6$ between Class II and Class III objects is also shown (*dash-dotted line*). Objects with Hα detected in absorption are shown as diamonds.

IfAHα 130 and IfAHα 141.—Herbig & Reipurth (2008) mention these as two objects with unusual spectra, combining aspects of the spectra of Herbig-Haro objects with stellar features. IfAHα 130 (YSO 78) appears pointlike in our *Spitzer* images, but IfAHα 141 (YSO 88) is clearly extended with a nonsymmetric shape (see Fig. 8), as also is apparently true in the optical images of Herbig & Dahm (2002).

V1735 Cyg = Elias 1-12.—This is the brightest YSO in the northwest streamer and is YSO 31 in Table 5. At 70 μm this object is somewhat confused with another nearly equally bright 70 μm source about 30″ northeast of it, YSO 34, that is associated with the submillimeter source found by Sandell & Weintraub (2001). Interestingly, Evans et al. (1994) discovered a bipolar outflow centered on the area of this submillimeter source, long before the continuum source was discovered. In the 70 μm mosaic the two sources appear of roughly equal brightness as an elongated image. The fluxes listed in Table 5 at 70 μm were derived by a crude deconvolution of the image, and thus have relatively large uncertainties associated with them. In any case YSO 34 is clearly an extremely cold, embedded object.

5.2. *Comparison with Submillimeter Observations and Extinction Maps*

Figure 9 shows the positions of the YSOs identified here against 850 and 450 μm emission observed toward IC 5146 with SCUBA. The SCUBA data were obtained from the SCUBA Legacy Catalogue (for details, see Di Francesco et al. 2008, in press). SCUBA data were only extant for the northwest streamer of IC 5146 and not the core region; both regions are expected to be observed at both 850 and 450 μm to higher sensitivity as part of the JCMT "Gould Belt" Legacy Survey (see Ward-Thompson et al. 2007).

Class I objects in the northwest streamer appear associated only with locations of bright dust emission at both 850 and 450 μm. Three such objects, including V1735 Cyg (Elias 1-12), are found in close proximity at the eastern end of the streamer, while two further Class I objects are found along or at the western end of the streamer. A sixth Class I object is associated with a thin filament of 850 μm emission to the north of the streamer. Interestingly, several (6–7) locations of dust emission along the streamer appear devoid of young stellar objects, and these knots may indicate sites of future star formation in the streamer, i.e., starless or prestellar cores. (Two other class I objects are located just at the eastern extreme of the SCUBA map area, where detection of dust emission is hardest to discern.)

YSOs in later evolutionary stages are also associated with the northwest streamer. One "flat-spectrum" object is seen just to the east of the dense grouping of Class I objects at the eastern end of the streamer. Also, six Class II objects are identified along the streamer (a seventh is likely also associated but is at the map edge.) Only one Class III object is associated with the streamer,

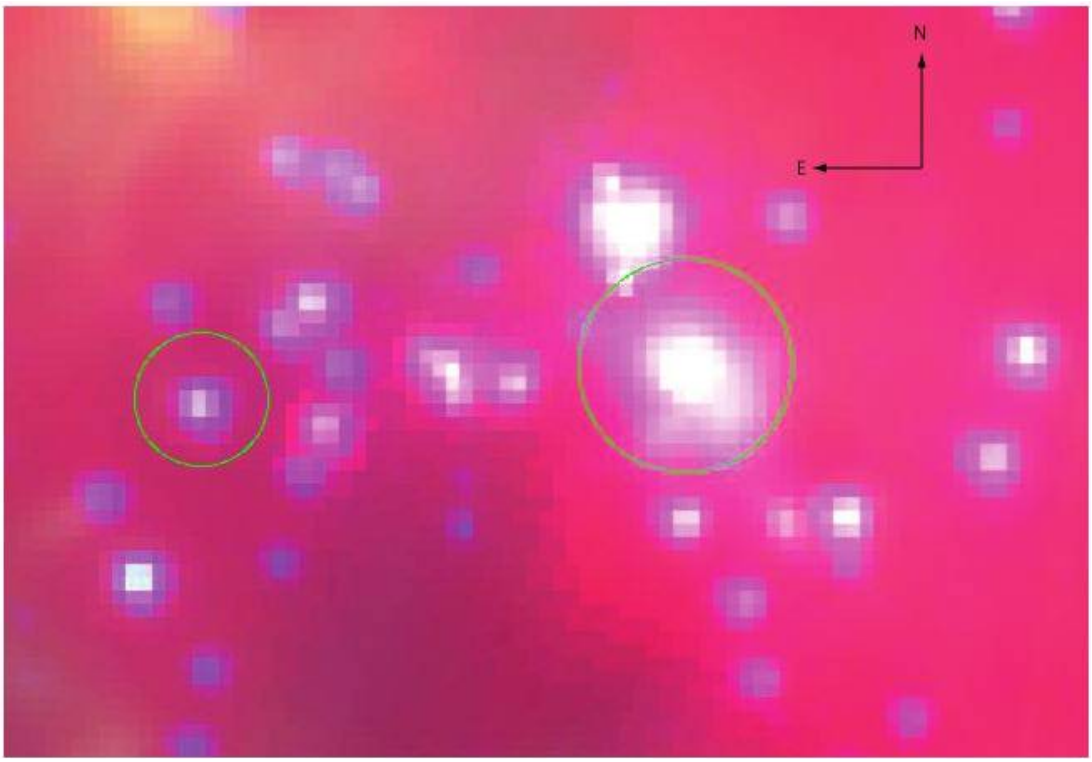

FIG. 8.—Area of $1' \times 1.5'$ in the center of the H II region showing the two objects with nonstellar images. BD +46 3474 is the object surrounded by nebulosity in the right half of the image and IfAHα 141 is the circled object in the left half of the image that is elongated north-south. In this image the 4.5 μm data are coded as blue, the 8.0 μm data as green, and the 24 μm data as red.

$\sim 1'$–$2'$ north of its middle. Unlike the Class I objects, the Class II and III objects appear less coincident with bright dust emission in the streamer, often appearing only nearby such emission. In addition, the Class II objects do not appear preferentially north or south of the streamer, although there are only relatively few such objects.

The only other identified objects within the area mapped by SCUBA include one Class II object and one Class III object, located $\sim 12'$ north of the filament. Unlike all other objects identified in this area, no submillimeter emission from dust is detected toward or near these objects.

In § 8.1 we present extinction maps derived from our data. In the region of overlap with the SCUBA data, there is excellent qualitative correspondence between regions of strong submillimeter emission and high derived extinction. We have also compared our extinction values with those from Cambrésy (1999). The relative changes in extinction show good correlation but the absolute value of the extinction derived from our infrared photometry is typically 2–5 times that derived by Cambrésy (1999) from optical data. This, of course, is to be expected since our measurements preferentially sample more obscured regions by being sensitive to more highly extincted stars.

6. DISK PROPERTIES: SED MODELING

Harvey et al. (2007) and Alcala et al. (2008) have discussed several methods to model the circumstellar disks believed to be responsible for most of the infrared excess emission in the Class II and Class III sources in the c2d data set. We have basically followed the approach of Harvey et al. (2007). We expect these objects to have a reddened photosphere plus an infrared excess coming from the circumstellar material, most likely in a disk configuration and have modeled them as such; for completeness we also show, without modeling, the SED's of the remaining YSOs. Figures 10–15 show the SEDs of all Class I, Class Flat, Class II, and Class III sources. The open dots are the observed fluxes and generally include 2MASS *J*, *H*, and *K* fluxes followed by the four IRAC fluxes at 3.6, 4.5, 5.8, and 8.0 μm and by the MIPS fluxes at 24 and 70 μm when available. We have also included optical fluxes from Herbig & Dahm (2002) or, if not observed by them, from the USNO NOMAD catalog (Zacharias et al. 2004). For the Class IIs and Class IIIs, we characterize the emission from the disk by comparing the energy distribution with that of a star. The only significant difference between our fitting and that described by Harvey et al. (2007) is that, because of the greater distance of IC 5146 and correspondingly higher typical stellar luminosity, we considered two possible underlying stellar photospheric distributions. We tried fits with either a K7 star or an A0 stellar photosphere (Hauschildt et al. 1999). We typically tried a K7 spectrum first, and where this showed a poor fit at the shortest wavelengths, then used the A0 spectrum instead. Figures 12–15 show that although this use of only two possible stellar models is clearly a huge oversimplification, it was, in fact, possible to get reasonable fits to most of the SEDs with this crude approximation. Clearly, the best approach is to obtain accurate spectral types at optical wavelengths for all the YSOs possible and perform a careful modeling of each object. That is beyond the scope of our present study, but we believe the rough statistical results we present are still of interest for comparison with YSOs in other star-forming regions. The dashed line in the SED plots is the median SED of T Tauri stars in Taurus (Hartmann et al. 2005) normalized to the dereddened *J*-band flux of our SEDs. It represents the typical SED of an optically thick accreting disk around a Classical T Tauri star and is shown here to allow a qualitative estimation of the presence of disk evolution and dust settling.

The SEDs and our simplified models allow several comparisons of overall disk properties with disks around YSOs in other

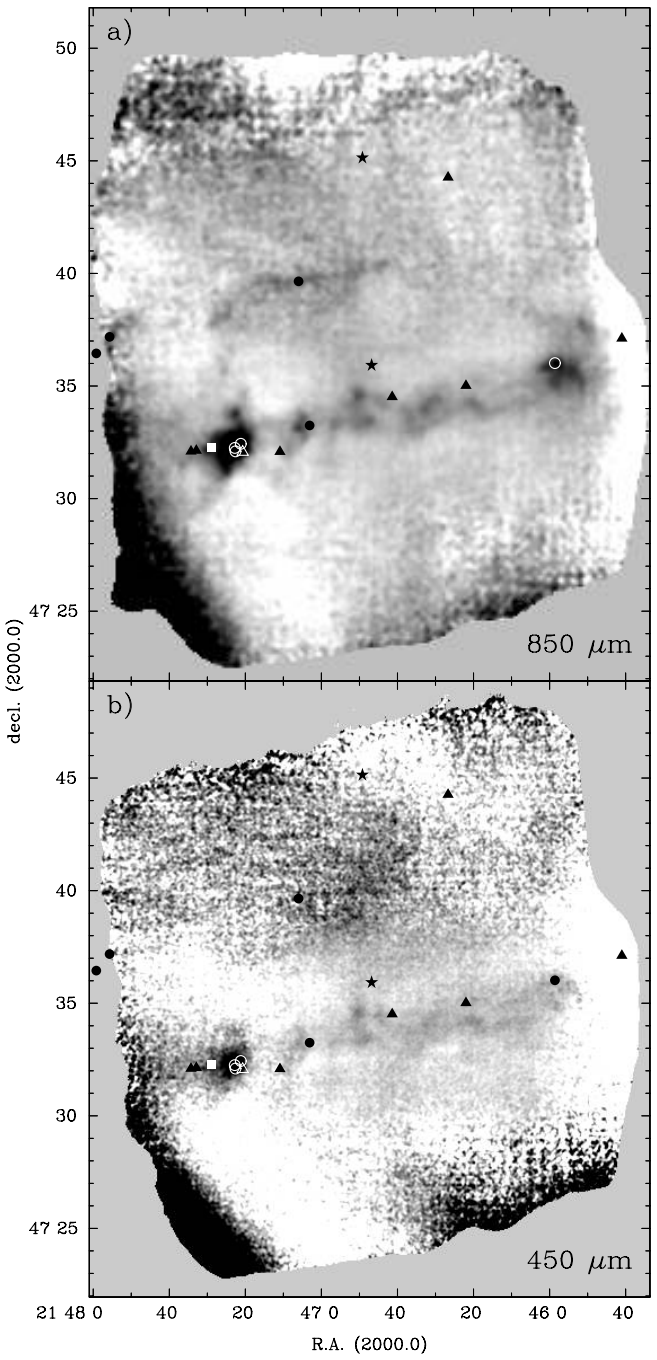

FIG. 9.—YSOs identified from *Spitzer* observations overlaid onto submillimeter continuum observations of the IC 5146 "streamer" from SCUBA. (Only a portion of the northwest streamer was observed with SCUBA.) The positions of Class I, "flat-spectrum," Class II, and Class III objects are identified, respectively with circles, squares, triangles, and stars. In panel *a*, 850 μm emission is shown in gray scale with a range of -0.1 to 0.3 Jy beam^{-1}. In panel *b*, 450 μm emission is shown in gray scale with a range of -0.5 to 2.0 Jy beam^{-1}.

star-forming clouds observed with *Spitzer*. First, we integrated the stellar and total fluxes to calculate a ratio between the stellar and the disk fluxes. The corresponding distribution is shown in Figure 16. To guide the eye, we have marked the approximate regimes of these ratios measured in debris disks ($L_{\rm disk}/L_{\rm star} < 0.02$), passive disks ($0.02 < L_{\rm disk}/L_{\rm star} < 0.08$, and accretion disks ($L_{\rm disk}/L_{\rm star} > 0.1$), respectively (e.g., Kenyon & Hartmann 1987). The figure illustrates well the large variety of disk evolutionary phases that we observe in IC 5146. The peak of this distribution is at log ($L_{\rm disk}/L_{\rm star} \sim 0.5$ implying that the typical disk has about one-third the stellar luminosity. This is quite similar to results found in studies from the c2d program for Serpens (Harvey et al. 2007), Chamaeleon II (Alcala et al. 2008), and Lupus (Merín et al. 2008). The second disk diagnostic we discuss has been developed to provide a more detailed characterization of disk evolutionary status than the venerable Class system. We use $\alpha_{\rm excess}$ and $\lambda_{\rm excess}$, two new *second-order* SED parameters presented in Cieza et al. (2007) and Harvey et al. (2007). In short, $\lambda_{\rm excess}$ is the last wavelength where the observed flux is photospheric and $\alpha_{\rm excess}$ is the slope computed as $d\log(\lambda F_\lambda)/d\log(\lambda)$ starting from $\lambda_{\rm excess}$. The first parameter gives us an indication of how far the circumstellar matter extends inward to the central object, and the latter one is a measure of how optically thick it is. Given the assumptions above for the fitting process, our values are upper limits for $\lambda_{\rm excess}$, and correspondingly lower limits for $\alpha_{\rm excess}$ for the Class II YSOs. Figure 17 shows values for our sample of YSOs in IC 5146, and Tables 10 and 11 list the values for each of the Class II and III sources, as well as other parameters of the fitted models. Cieza et al. (2007) found that $\lambda_{\rm excess}$ is well correlated with evolutionary phase and also, as seen in Figure 17, that α is observed over wider ranges for later evolutionary phases. This is also consistent with the distribution of α with $\lambda_{\rm excess}$ seen for YSOs in Serpens by Harvey et al. (2007). We note the two objects in the upper right part of this diagram, YSOs 13 and 102, would be classified as "transition disks" in recent terminology. More generally, the objects with the lowest ratios of disk to stellar luminosity in Figure 16 are those in the rightmost two bins of $\lambda_{\rm excess}$ in Figure 17.

7. DISK FRACTION

As noted numerous times by investigators from the c2d team with observations similar to ours, YSOs found by *Spitzer* are by their nature those with infrared excesses due to emission from surrounding dust, either in disks and/or envelopes. The population of diskless, e.g., Lada Class III, sources is by and large rejected by our selection criteria unless there is some small remnant IR excess. There is, however, a way to use *Spitzer*'s exquisite sensitivity in the low extinction infrared to measure in a statistical sense the YSO population in a cluster. Gutermuth et al. (2005) and references therein, for example, have discussed a technique based on comparing the source counts in "cluster" regions to off-cluster areas. Their technique has largely used observations in the *K* band. In our case, the most sensitive band for detecting faint stars is IRAC band 1 at 3.6 μm, since our *K* data are limited by the 2MASS sensitivity.

To use this technique we have identified regions in our maps of high YSO density and much lower or zero density (see § 8.1). Figures 18 and 19 show the "on-cluster" and "off-cluster" areas for both the IC 5146 central core and the northwest streamer superimposed on the extinction maps discussed later in § 8.1. In each marked region we have measured the median extinction and the star counts for both all catalogued IC 5146 objects at 3.6 μm, as well as the YSOs identified in any of Tables 5, 6, and 7. We then produced differential star count figures for the on- and off-cluster areas as well as a calculation from the Wainscoat models (Wainscoat et al. 1992) of the expected star counts in those directions assuming the measured extinction differential between the on- and off-cluster regions. Figures 20 and 21 show these results. For both regions there is good agreement of the model counts and the off-cluster region counts within the statistical uncertainties. For the eastern "core" region, there is clearly an excess of star counts over a wide range of magnitudes, but for the northwest streamer there is no significant excess. The lower panel of each figure shows the actual count difference between the

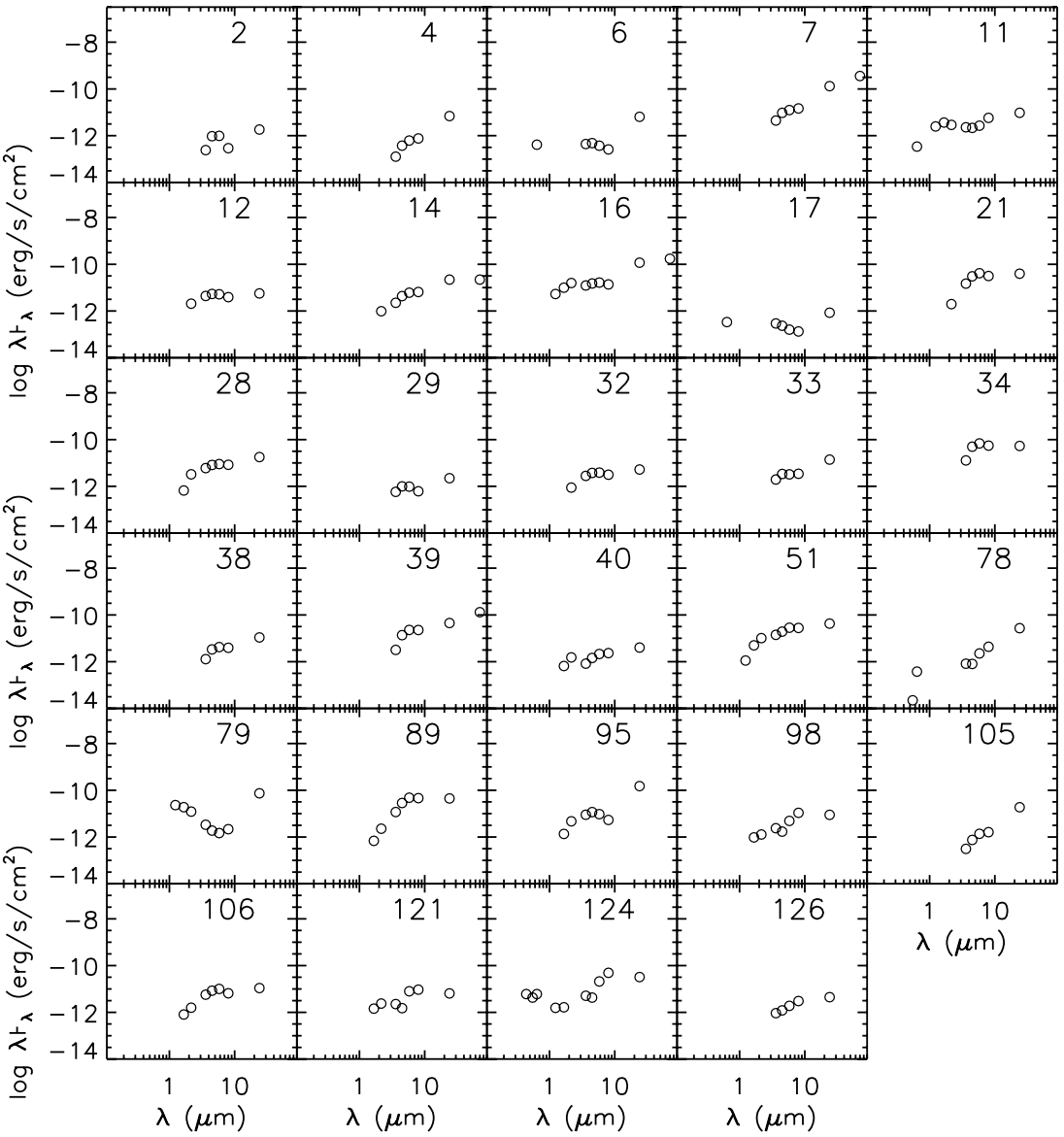

FIG. 10.—SEDs of the YSOs from Table 5 that have spectral slopes characteristic of Class I sources. The numbers in each figure refer to the numbers in Table 5.

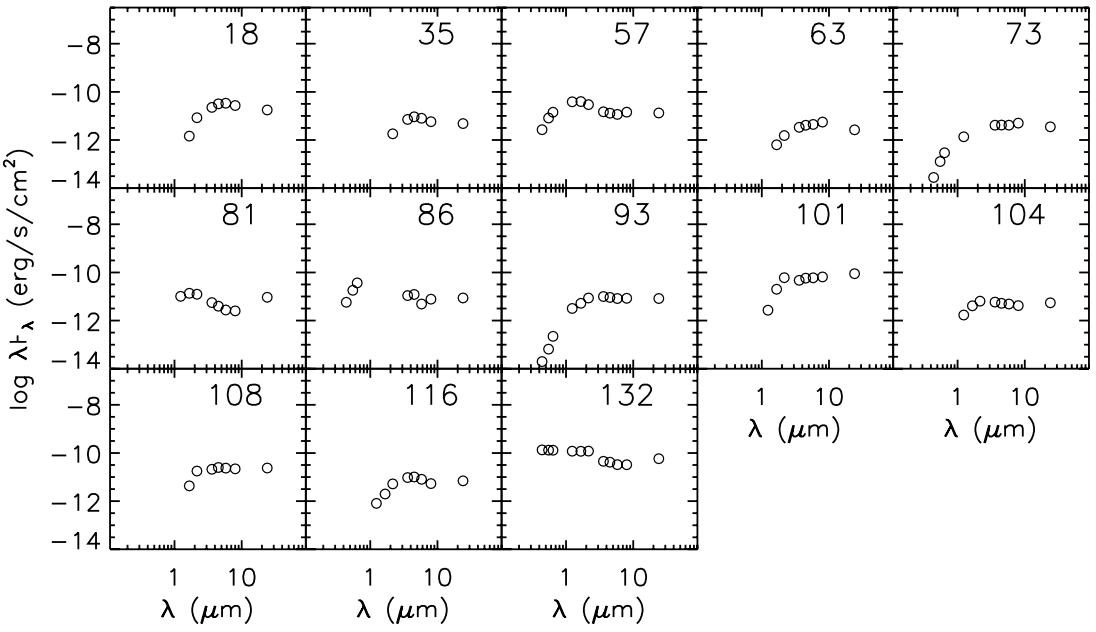

FIG. 11.—SEDs of the YSOs from Table 5 that have spectral slopes characteristic of flat-spectrum sources as in Fig. 10.

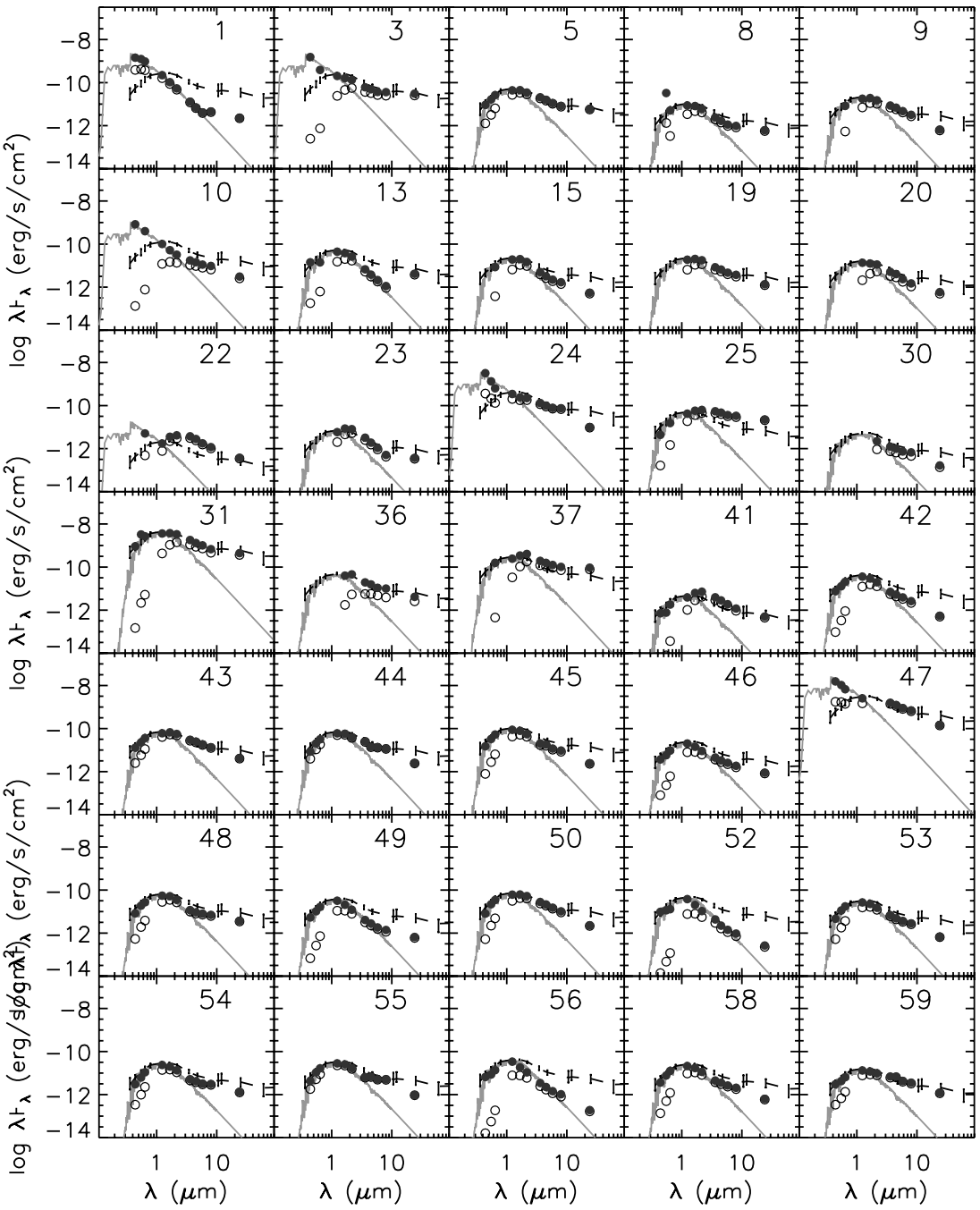

FIG. 12.—SEDs of the YSOs from Table 5 that have spectral slopes characteristic of Class II sources as in Fig. 10. In addition to the measured fluxes (*open circles*), we also show the dereddened fluxes (*filled circles*) derived from the SED-fitting procedure described in the text, as well as the photospheric SED used to fit the shorter wavelength points (*solid line*). The dashed line is the median SED of T Tauri stars in Taurus (Hartmann et al. 2005).

on- and off-cluster regions normalized to the total on-cluster area. The counts for the core cluster region show an additional effect in a deficit in counts at magnitudes fainter than 16.5 relative to the off-cluster regions. It is likely this is due to the level of nebulosity, even at 3.6 μm, in this region, which is limiting our ability to extract the faintest sources from the image. It appears from the crossover of the count distributions at $[3.6] \sim 15.5$, that this effect probably becomes significant for $[3.6] > 15.0$. We also looked at the two on-cluster regions individually in Figure 18. Within the statistical uncertainties, both regions showed comparable excess counts relative to the off-cluster regions. The westernmost of the two, however, which does not include any of the obvious nebulosity, did not exhibit the deficit in counts at fainter magnitudes. This is clearly consistent with our hypothesis that the deficit is caused by our inability to detect faint objects in the presence of the nebulosity.

In order to estimate the ratio of total YSOs to those found by *Spitzer*, we need to estimate the completeness limit of our *Spitzer* YSO sampling. This is not the same as the survey completeness limit. As described by Harvey et al. (2007) in Serpens, there is good evidence that fainter YSOs are filtered out by our strong selection criteria aimed at eliminating extragalactic contamination. Indeed, Figure 22 shows the histogram of 3.6 μm magnitudes for the sample of five-band YSOs in Table 5 and also for

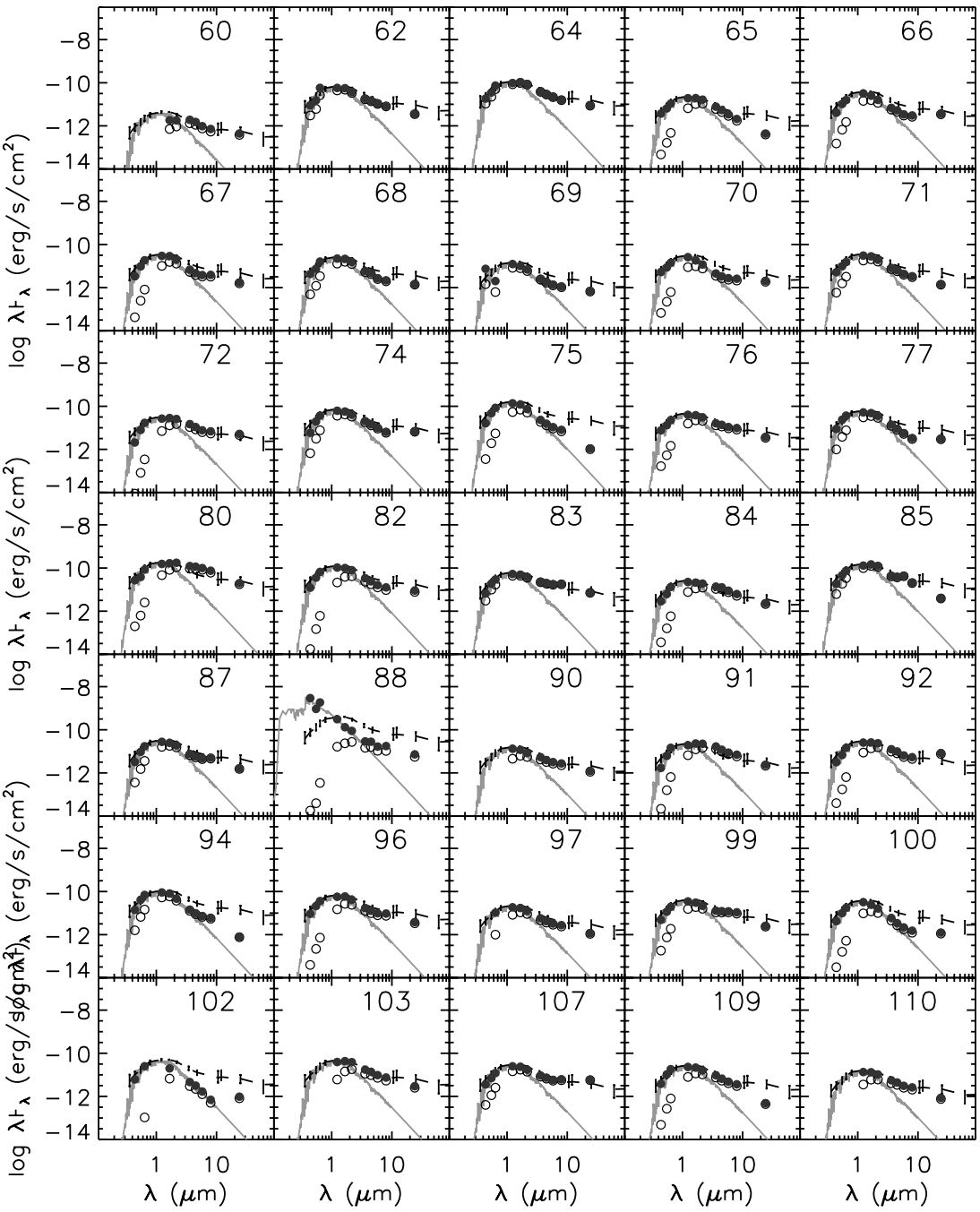

FIG. 13.—SEDs of the YSOs from Table 5 that have spectral slopes characteristic of Class II sources as in Fig. 12.

the "IRAC-only" ones in Table 7. Even though our survey completeness limit from Figure 20, for example, appears to be of order $[3.6] < 16$ (with the limitations discussed above for $[3.6] > 15$), it is clear that our ability to find YSOs becomes severely limited at magnitudes fainter than $[3.6] \sim 12.5$.

Table 12 lists the various statistics relevant to estimating the ratio of YSOs with and without IR excesses in the IC 5146 core region for two choices of the limiting YSO magnitude, 15.0 and a more realistic value of 12.5. The most reliable estimate of the ratio of YSOs with detectable IR excess to those without is probably the ratio for sources brighter than $[3.6] < 12.5$. Using this cutoff, the ratio is $N_{\rm disk}/N_{\rm total} \sim 0.5$–$0.6$ (somewhere between 70 and 90 YSOs with disks out of 140 total objects in excess of the background star counts), depending on how many of the IRAC-only and MIPS-only YSOs are real. Thus the number of disk-less YSOs in this magnitude range is probably of order 60. In § 8.1 we present a similar analysis using Wainscoat (Wainscoat et al. 1992) model counts instead of actual number counts to estimate the total cluster membership. In that case we estimate $N_{\rm disk}/N_{\rm total} \sim 0.4$. Table 12 also shows, however, that the number of missed YSOs at the faint end is likely to be quite significant. If we assume that the same ratio of disked to diskless YSOs applies down to $[3.6] \sim 15$, then we would expect of order 200–250 YSOs in the core cluster alone! If they are there, many of them are of course too faint at longer wavelengths to be detected at our sensitivity levels with the modest integration times used for this survey. More importantly,

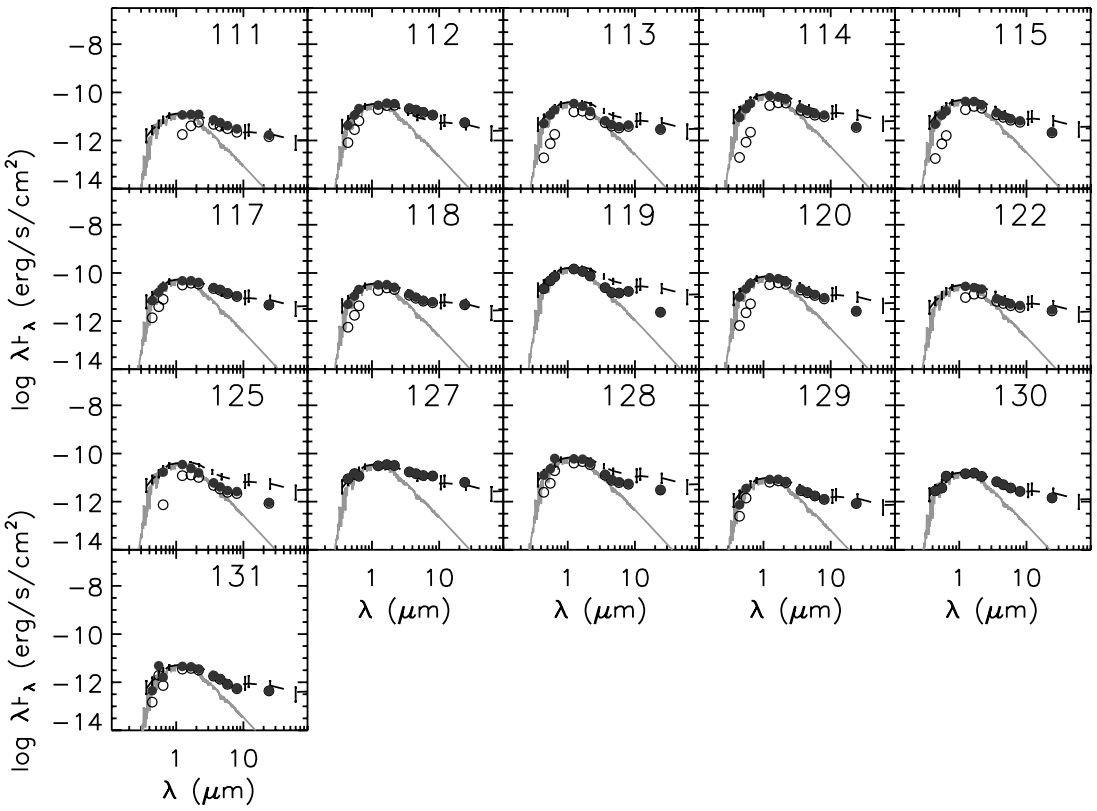

FIG. 14.—SEDs of the YSOs from Table 5 that have spectral slopes characteristic of Class II sources as in Fig. 13.

even if they were detected, it would be *very* difficult to distinguish them from extragalactic contaminants without additional data at other wavelengths, and/or follow-up spectroscopy.

The fraction of cluster members with disks that we derive, of order 50%, is noticeably less than that in several other young clusters, 65% in IC 348 (Haisch et al. 2001), 86% in NGC 2024 (Haisch et al. 2000), and 80% for the Trapezium (Lada et al. 2000). This suggests that the age of this cluster may be somewhat older than any of those others, i.e., perhaps several Myr, although Herbig & Dahm (2002) estimated a median age of 1 Myr from the optical main sequence in the core cluster, and the photometry discussed above relevant to the distance (§ 2) is consistent with an age under 1 Myr.

8. OVERALL CLOUD STRUCTURE AND SOURCE DISTRIBUTION

8.1. *Extinction, YSO Clustering, and Star Formation Efficiency*

It is possible to investigate the spatial relationship of the young stars and the material from which they formed using only our *Spitzer* data. Part of the process of band-merging in the c2d pipeline (see footnote 11) involves classifying the SED of each source. One possible class is a reddened stellar photosphere. There are more than 30,000 such objects in our IC 5146 source catalogs, which makes it possible to derive an estimate of the visual extinction from *Spitzer* data alone over our whole mapped area. Since most of this extinction is due to material local to the star-forming region, we can also use it to estimate the distribution of that local material.

For direct comparisons to the clouds studied by c2d (see, e.g., Alcala et al. 2008), we identified substructure in the distribution of YSOs in IC 5146 using a nearest neighbor algorithm (Jørgensen et al. 2008). Briefly, we roughly follow Gutermuth et al. (2005) by calculating surface and volume densities at each position using the distance to the fifth-nearest neighbor as a sample size from which to calculate the local stellar density. We estimate the volume density assuming that the distribution of YSOs is locally spherically symmetric. Following the discussion by Jørgensen et al., we identify structures with mass volume densities higher than 1 $M_{\odot}$ pc^{-3} (similar to the criterion for a cluster by Lada & Lada, 2003; "1 × LL03" in the following) and 25 $M_{\odot}$ pc^{-3} (25 × LL03 in the following) as being "loose" or "tight," respectively.

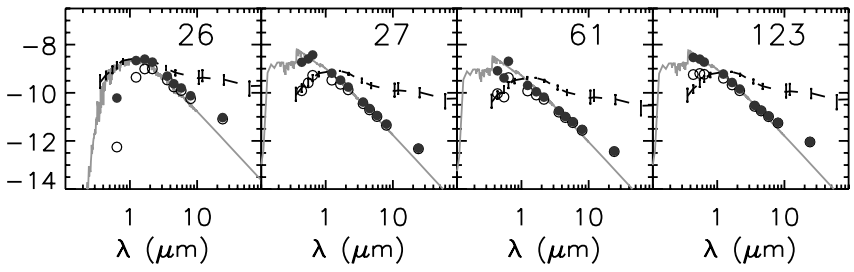

FIG. 15.—SEDs of the YSOs from Table 5 that have spectral slopes characteristic of Class III sources as in Fig. 12.

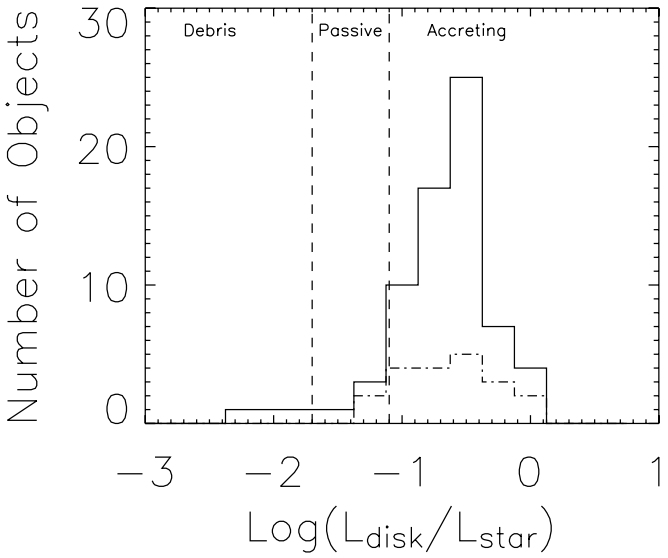

FIG. 16.—Distribution of disk to star luminosity ratios. The solid and dashed lines are the distributions for the IC 5146 core region and for the northwest streamer, respectively. Also marked are the typical ranges of $L_{\rm disk}/L_{\rm star}$ ratios for debris disks, passive irradiated disks, and accretion disks. The figure indicates that objects of all three evolutionary stages are found in IC 5146, with a predominance of young accreting T Tauri type stars.

For an average stellar mass of 0.5 $M_{\odot}$ this corresponds to number volume densities of two YSOs pc^{-3} and 50 YSOs pc^{-3}, respectively. These concentrations of YSOs are furthermore divided into "clusters" or "groups" depending on whether they have more or less than 35 members at a given volume density level.

Figure 23 shows the volume density contours for IC 5146 assuming a distance of 950 pc for the 5-band YSOs in Table 5. We have included only the 5-band YSOs in this analysis because they are considerably more reliable than the *candidates* identified from either the IRAC-only or MIPS-only data. Three separate loose concentrations of YSOs are clearly identified across the cloud in both figures. In addition, there are clearly several YSO candidates associated with dense material at the edges of our maps, but since we did not cover the entire likely area of those clusters, we cannot include them in this analysis. Most (85%) of the YSOs in the "core" are located within the boundary of a loose cluster which at the higher $25 \times$ LL03 level breaks into two tight groups also clearly identifiable by eye. The YSOs in the Northwest streamer fall into two clearly separated groups. The easternmost, "B", contains eight YSOs and the westernmost, "C", has 13 YSOs. Close to half of the YSOs in the streamer, however, are found in isolation, i.e., not associated with these two groups.

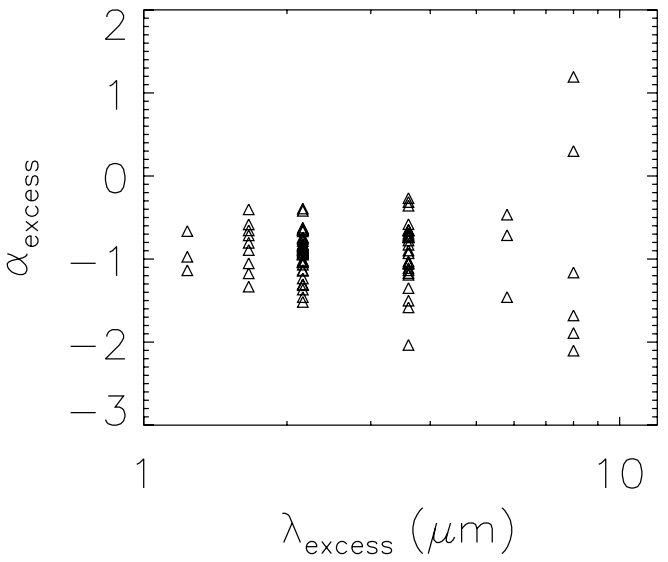

FIG. 17.—Distribution of excess slopes $\alpha_{\rm excess}$ with respect to the wavelength at which the infrared excess begins $\lambda_{\rm turnoff}$ for the Class II and Class III sources in IC 5146. The diagram shows a much larger spread in inner disk morphologies in the more evolved objects than in the least evolved ones as seen in other star-forming regions as well.

TABLE 10
DISK MODELING RESULTS IN CLASS II SOURCES

Star	A_V	log ($L_{\rm star}$)	$L_{\rm disk}/L_{\rm star}$	$\lambda_{\rm turnoff}$	$\alpha_{\rm excess}$	Spectral Type
1.....	1.2	1.66	0.10	5.8	−0.5	A0
3.....	8.0	1.63	0.11	1.7	−0.7	A0
5.....	1.8	0.23	0.48	2.2	−0.7	K7
8.....	3.5	−0.47	0.45	3.6	−0.7	K7
9.....	3.5	−0.15	0.43	2.2	−1.3	K7

NOTE.—Table 10 is published in its entirety in the electronic edition of the *Astrophysical Journal*. A portion is shown here for guidance regarding its form and content.

Using the boundaries of each of these groups we estimate the mass within each region from the extinction maps (made with 240″ resolution with the method described in Harvey et al. (2007) and shown in Figures 18 and 19) and calculate the corresponding star formation efficiencies (SFEs) from

$$\mathrm{SFE} = \frac{M_{\rm YSO}}{M_{\rm YSO} + M_{\rm dust+gas}},$$

where $M_{\rm YSO}$ is the total mass of the YSOs (the number of YSOs times 0.5 $M_{\odot}$) and $M_{\rm cloud}$ the total gas+dust mass within the volume density contour. The stellar mass is clearly a lower limit, since we estimate that our YSO detection process becomes significantly incomplete below 0.5–1 $L_{\odot}$. The gas mass was estimated assuming the standard ratio of gas column density to extinction (Bohlin et al. 1978), 9.4×10^{20} cm^{-2} mag^{-1}. Since the ratio of gas column density to extinction may be higher in dense regions, these estimates are likely to be lower limits also. We integrated the inferred H_2 column density inside various surface/volume density contours and multiplied by the molecular weight per hydrogen molecule, 2.8. Finally, we estimate the number of anticipated diskless YSOs from the number of stars detected at 3.6 μm. From the Wainscoat models a total of 202 stars deg^{-2} with $[3.6] < 12$ are expected toward IC 5146. By taking the actual area of each group or cluster into account we can estimate the number of stars toward each region which in turn can be subtracted from the actual

TABLE 11
DISK MODELING RESULTS IN CLASS III SOURCES

Star	A_V	log($L_{\rm star}$)	$L_{\rm disk}/L_{\rm star}$	$\lambda_{\rm turnoff}$	$\alpha_{\rm excess}$	Spectral Type
26.....	6.0	1.93	0.18	3.6	−2.0	K7
27.....	2.5	2.13	0.18	8.0	−2.1	A0
61.....	2.0	1.84	0.19	8.0	−1.9	A0
123.....	1.5	2.09	0.01	8.0	−1.7	A0

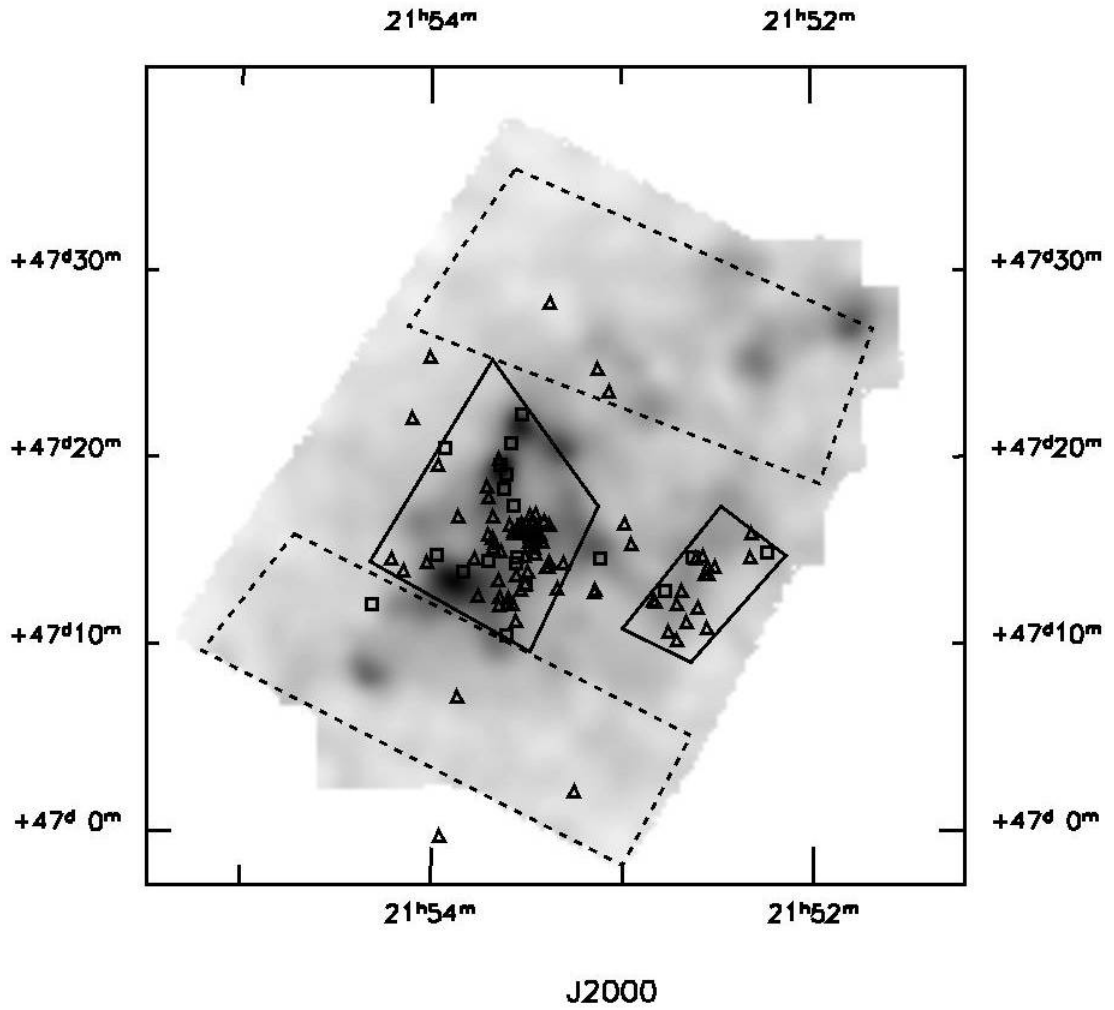

FIG. 18.—Locations of the on-cluster (*solid line*) and off-cluster (*dashed line*) areas selected in the IC 5146 core cluster region for comparison of star counts, superimposed on the extinction (*gray scale*) derived from our standard data processing that fits extinction and photospheric fluxes to objects that appear to be reddened stellar photospheres. The extinction ranges from $A_V \sim 1.5$ in the lightest areas to 15 in the darkest regions. The locations of the YSOs from Tables 5, 6, and 7 are also marked with triangles representing the Class II and III sources, and squares representing the Class I and flat SED sources.

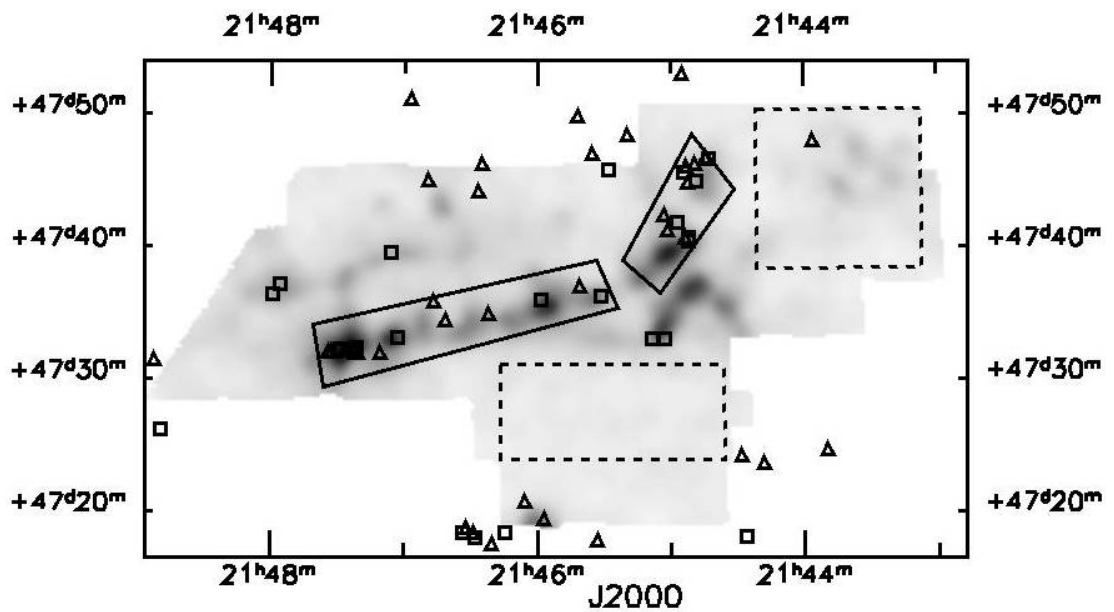

FIG. 19.—As for Fig. 18 for the area of the northwest streamer. In this region the extinction ranges from $A_V \sim 2.5$ in the lightest areas to 30 in the darkest regions.

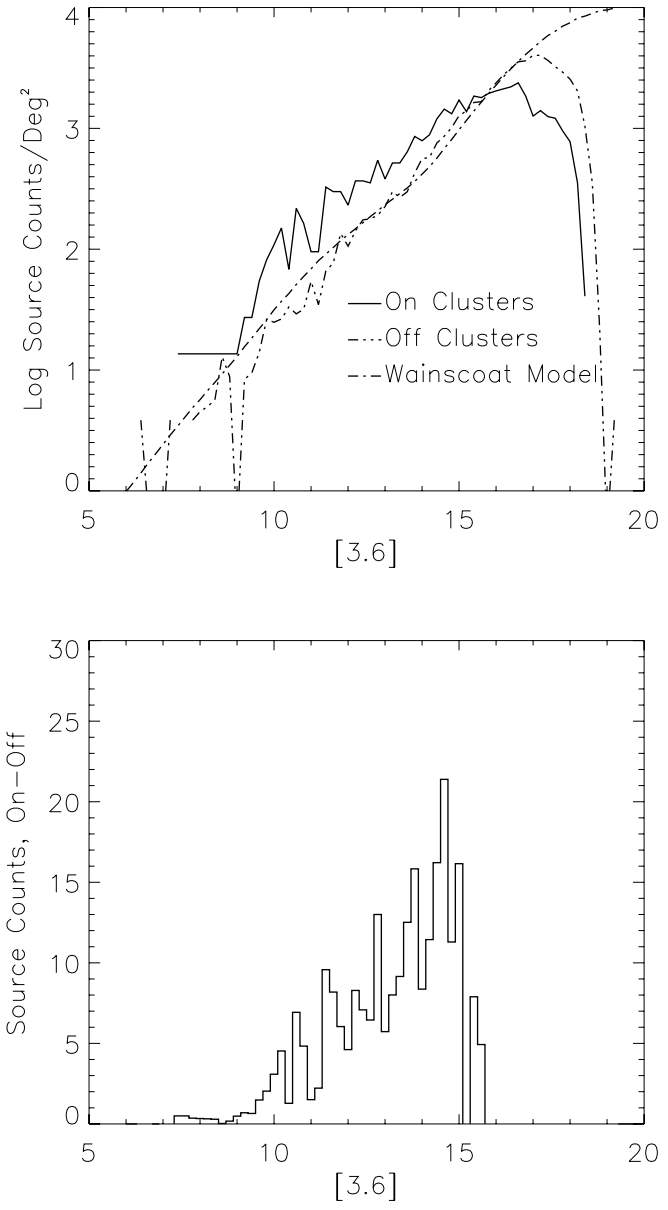

FIG. 20.—*Top*: Differential source counts at 3.6 μm for the "core" cluster region of IC 5146. The solid line shows the counts for the combination of the two on-cluster areas; the dashed line shows the same for the sum of the two off-cluster regions; the smooth dash-dot line shows the prediction from the Wainscoat model for this direction in the Galaxy. *Bottom:* Difference in counts for the sum of the two on-cluster regions, i.e., on − off cluster counts normalized to the total of the two on-cluster areas in Fig. 18.

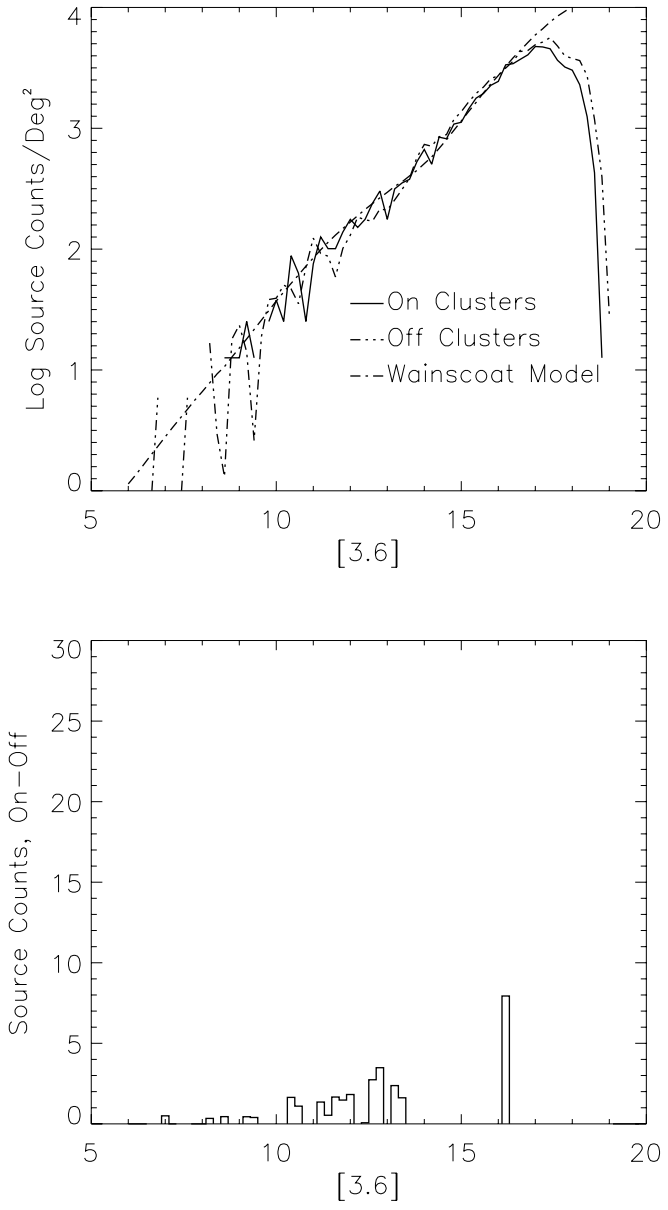

FIG. 21.—As for Fig. 20 for the northwest streamer region. This figure shows that there is no detectable excess of counts in the on-cluster regions relative to the off-cluster ones.

number of stars observed. This gives a measure of the fraction of YSOs which are so evolved that no significant infrared excess emission is observed as discussed also in § 7.

Table 13 summarizes the number of YSOs in each of the concentrations in IC 5146 together with their average extinctions, star formation efficiencies and the fraction of sources without disks relative to those with disks. Again, it is striking to note the differences in the number of embedded YSOs (e.g., Class I) relative to overall YSOs between the groups in the core and in the northwest streamer. Similar large differences are seen in clouds such as Perseus: the fraction of Class I sources in the core region (about 10%) is similar to that of the IC 348 cluster in that cloud whereas the fractions in the regions in the streamer compare better to the NGC 1333 cluster and the smaller B1, L1448, and L1455 groups in Perseus (e.g., Jørgensen et al. 2006

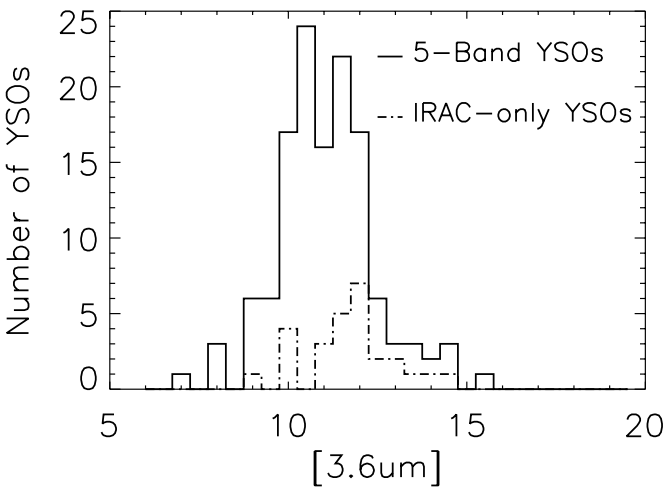

FIG. 22.—Histogram of the number counts vs. [3.6] for the five-band YSOs from Table 5 and the IRAC-only YSOs from Table 7.

TABLE 12

STAR COUNT STATISTICS FOR THE CORE CLUSTER

Statistic	On-Cluster	Off-Cluster[a]	On − Off
Median extinction (A_v)	6.54	2.84	3.7
Source counts, [3.6] < 15	922	492	430
Source counts, [3.6] < 12.5	213	71	142
YSO counts, [3.6] < 15	97	2	95
YSO counts (five-band), [3.6] < 15	81	2	79
YSO counts, [3.6] < 12.5	91	2	89
YSO counts (five-band), [3.6] < 12.5	75	2	73

[a] Counts normalized to on-cluster area for comparison.

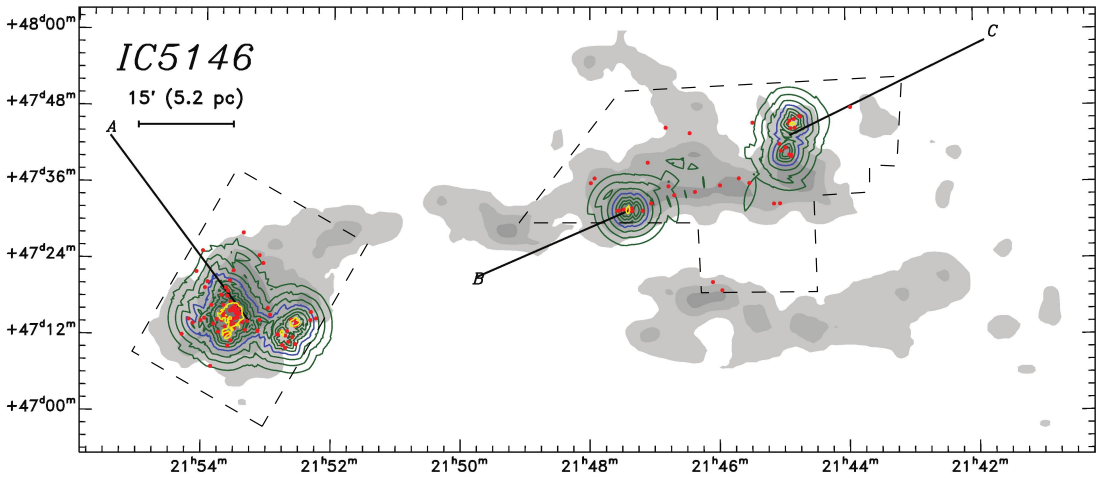

FIG. 23.—Volume density contours of the five-band YSOs in IC 5146 from Table 5 assuming a distance of 950 pc shown on top of extinction maps (Cambrésy 1999; *gray scale*). The green contours indicate the volume densities corresponding to 12.5%, 25%, 50%, 200%, and 400% the criterion suggested by Lada & Lada (2003) of 1 $M_\odot$ pc^{-3} (1 × LL03). The blue contours indicate the volume density corresponding to this criterion, and the yellow contours correspond to volume densities 25 times higher than this level. The red dots show the location of the YSOs in the cloud. The approximate areas of full five-band coverage are shown by the dashed lines, as well as shown exactly in Figs. 2 and 3.

TABLE 13

CLUSTERING ANALYSIS FOR IC 5146

Cluster	Type	Number of YSOs	I	Flat	II	III	$\langle A_v \rangle$ (mag)	Mass ($M_\odot$)	Volume (pc^3)	SFE[a] (%)	$n_{\rm nodisk}/n_{\rm YSO}$
Total		132	29 (22%)	12	87	4	...	13452	...	0.49	...
A	LC	79	10 (13%)	8	61	0	6.0	1309	25.5	2.9	1.84
Tight east	TG	29	3 (10%)	2	24	0	7.7	134.3	0.564	9.7	1.74
Tight west	TG	5	0 (0%)	0	5	0	4.8	10.31	0.0246	20	1.38
B	LG	8	3 (38%)	1	4	0	11.3	437.5	1.88	0.90	1.58
C	LG	13	5 (38%)	1	7	0	6.6	376.8	3.39	1.7	1.23
Distributed		32	11 (34%)	2	15	4	...	...	...	...	...

[a] SFE defined as SFE = $(0.5\ M_\odot N_{\rm YSOs})/(0.5\ M_\odot N_{\rm YSOs} + M_{\rm dust+gas})$.

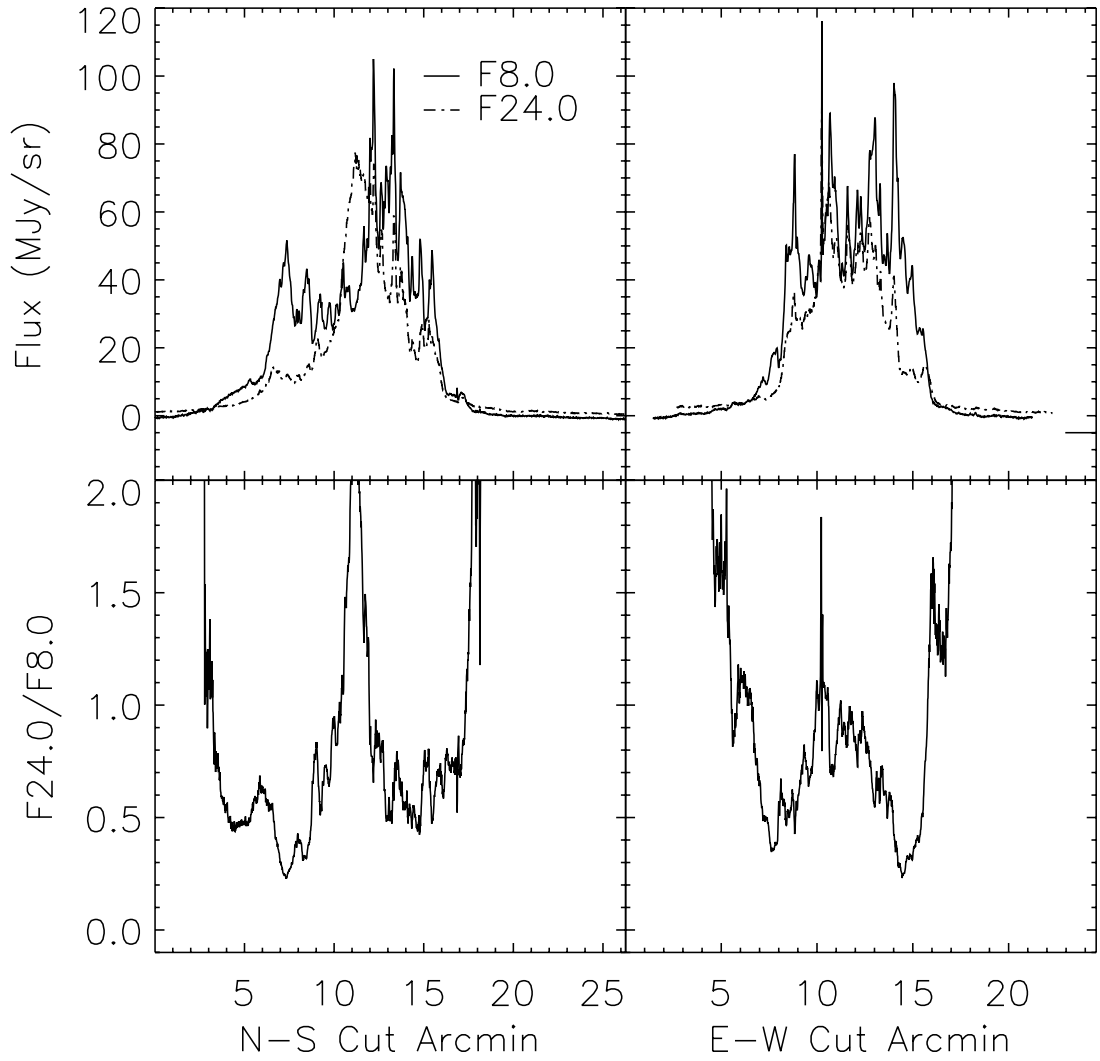

FIG. 24.—Plots of the 8.0 and 24 μm surface brightness through the center of the IC 5146 diffuse nebulosity. The top panels show the flux at both 8 and 24 μm, and the bottom panels show the ratio of the two. The locations of the two spatial cuts are indicated on Fig. 2.

and in preparation). In Perseus this has been interpreted to reflect differences in ages between the different subregions with typical age estimates for IC 348 of 2–3 Myr compared to $\lesssim$1 Myr for NGC 1333.

8.2. *Diffuse Extended Emission*

The large amount of substructure in the diffuse emission around the core of IC 5146 makes it difficult to discern any large scale trends. In Figure 24, however, we have plotted the 8 and 24 μm surface brightness across a north-south and east-west cut through the image (indicated in Fig. 2), as well as the ratio of the two wavelengths. The overriding feature in these plots is the fact that the 24 μm emission peaks both at the center of the nebula and in the outer regions, while the 8 μm emission seems to peak at intermediate radii. This effect does not depend on the exact location of the cuts, i.e., it is a robust, large-scale effect. Presumably most of the 8 μm emission originates from PAH small-grain emission, while most of the 24 μm emission comes from larger and/or more uniformly heated grains.

Draine & Li (2007) have recently published results of detailed modeling of grain emission illuminated by a variety of UV fields. The sharp rise in 24 μm emission we see near the center of the nebula relative to the 8 μm emission can probably be explained by the nonlinear sensitivity of the 24 μm emission to UV heating in radiation fields of 10^4–10^5 times the normal interstellar field as illustrated in Figure 15 of their paper. The increase in the ratio of F_{24}/F_8 near the edges of the infrared nebulosity is more difficult to understand in detail. It may involve some combination of effects due to changing ionization conditions between the H II region and the photodissociation region beyond it, and/or to changing grain sizes between those two regions. Spatially resolved spectroscopy of the relative strengths of individual PAH features may be required to explain the structure we see.

9. SUMMARY

Using *Spitzer* IRAC and MIPS photometry we have identified $\sim$200 YSO candidates in the core region of IC 5146 around the H II region and the northwest streamer, one of the dark clouds likely to be physically associated with the H II region. We find substantial differences in the YSO population in the two separated areas: the population near the H II region is more evolved spectrally on the average, while that in the northwest streamer, although significantly less rich in total number, has a higher fraction of objects with Class I or flat SED's. One of the coldest, most embedded objects is associated with the submillimeter source found by Sandell & Weintraub (2001) near V 1735 Cyg (Elias 1-12) in

the northwest streamer. Our very crude modeling of the disk population around the Class II and III sources agrees with that from earlier *Spitzer* YSO population studies (e.g., Harvey et al. 2007) in that the more spectrally evolved sources with IR excesses that start only at longer wavelengths appear to show the most variation in amount of excess. We estimate the fraction of YSOs with disks in the core to be roughly 50% of the total YSO population, a value that suggests an older age for that cluster than some other estimates of less than 1 Myr. We have also estimated the star formation efficiency in various volumes of our YSO clusters using extinction results derived from our photometry to measure the gas mass. The values range from less than 1% for the region taken as a whole up to 20% for the highest density area.

Support for this work, part of the *Spitzer* Legacy Science Program in the GO3 call, was provided by NASA through contract 1288664 issued by the Jet Propulsion Laboratory, California Institute of Technology. This publication makes use of data products from the Two Micron All Sky Survey, which is a joint project of the University of Massachusetts and the Infrared Processing and Analysis Center/California Institute of Technology, funded by NASA and the National Science Foundation. We also acknowledge use of the SIMBAD database. E. E. M. is supported through a Clay Postdoctoral Fellowship from the Smithsonian Astrophysical Observatory.

Facilities: Spitzer

REFERENCES

Alcala, J., et al. 2008, ApJ, 676, 427
Aller, L. H., et al. 1982, Numerical Data and Functional Relationships in Science and Technology (Group 6), ed. H. Landolt & R. Börnstein (Berlin: Spinger)
Balona, L. A., & Feast, M. W. 1975, MNRAS, 172, 191
Barnard, E. E. 1919, ApJ, 49, 1
Blaauw, A. 1963, Basic Astronomical Data: Stars and Stellar Systems, ed. K. A. Strand (Chicago: Univ. Chicago Press)
Bohlin, R. C., Savage, B. D., & Drake, J. F. 1978, ApJ, 224, 132
Cambrésy, L. 1999, A&A, 345, 965
Cieza, L., et al. 2007, ApJ, 667, 308
Crampton, D., & Fisher, W. A. 1974, Publ. Dominion Astrophys. Obs. Victoria, 14, 283
D'Antona, F., & Mazzitelli, I. 1997, Mem. Soc. Astron. Italiana, 68, 807
Di Francesco, J., Johnstone, D., Kirk, H. M., MacKenzie, T., & Ledwosinska, E. 2008, ApJS, 175, 277
Dobashi, K., Uehara, H., Kandori, R., Sakurai, T., Kaiden, M., Umemoto, T., & Sato, F. 2005, PASJ, 57, 1
Dobashi, K., Yonekura, Y., & Hayashi, Y. 2001, PASJ, 53, 811
Dobashi, K., Yonekura, Y., Mizuno, A., & Fukui, Y. 1992, AJ, 104, 1525
Draine, B. T., & Li, A. 2007, ApJ, 657, 810
Elias, J. H. 1978, ApJ, 223, 859
Evans, N. J. II, Balkum, S., Levreault, R. M., Hartmann, L., & Kenyon, S. 1994, ApJ, 424, 793
Evans, N. J., II, et al. 2003, PASP, 115, 965
Forte, J. C., & Orsatti, A. M. 1984, ApJS, 56, 211
Greene, T. P., Wilking, B. A., André, P., Young, E. T., & Lada, C. J. 1994, ApJ, 434, 614
Gutermuth, R. A., Megeath, S. T., Pipher, J. L., Williams, J. P., Allen, L. E., Myers, P. C., & Raines, S. N. 2005, ApJ, 632, 397
Haisch, K. E., Lada, E. A., & Lada, C. J. 2000, AJ, 120, 1396
———. 2001, AJ, 121, 2065
Hartmann, L., et al. 2005, ApJ, 629, 881
Harvey, P. M., et al. 2006, ApJ, 644, 307
———. 2007, ApJ, 663, 1149
Hauschildt, P. H., Allard, F., Ferguson, J., Baron, E., & Alexander, D. R. 1999, ApJ, 525, 871
Herbig, G. H., & Dahm, S. E. 2002, AJ, 123, 304
Herbig, G. J., & Reipurth, B. 2008, in Handbook of Star-Forming Regions, ed. B. Reipurth (San Francisco: ASP), in press
Jaschek, C., & Gomez, A. E. 1998, A&A, 330, 619
Johnson, H. L., & Hiltner, W. A. 1956, ApJ, 123, 267
Johnson, H. L., & Morgan, W. W. 1953, ApJ, 117, 313
Jørgensen, J. K., et al. 2006, ApJ, 645, 1246
———. 2008, ApJ, submitted
Kenyon, S. J., & Hartmann, L. 1987, ApJ, 323, 714
Kramer, C., Richer, J., Mookerjea, B., Alves, J., & Lada, C. 2003, A&A, 399, 1073
Lada, C. J. 1987, in IAU Symp. 115, Star-Forming Regions, ed. M. Peimbert & J. Jugaku (Dordrecht: Reidel), 1
Lada, C. J., Alves, J., & Lada, E. A. 1999, ApJ, 512, 250
Lada, C. J., & Lada, E. A. 2003, ARA&A, 41, 57
Lada, C. J., Lada, E. A., Clemens, D. P., & Bally, J. 1994, ApJ, 429, 694
Lada, C. J., Muench, A. A., Haisch, K. E., Lada, E. A., Alves, J. F., Tollestrup, E. V., & Willner, S. P. 2000, AJ, 120, 3162
Lada, C. J., et al. 2006, AJ, 131, 1574
Littlefair, S. P., Naylor, T., Harries, T. J., Retter, S., & O'Toole, S. 2004, MNRAS, 347, 937
Lynds, B. T. 1962, ApJS, 7, 1
Martin, E. L. 1997, A&A, 321, 492
Menten, K. M., et al. 2007, A&A, 474, 515
Merín, B., et al. 2008, ApJ, in press (arXiv: 0803.1504)
Rebull, L., et al. 2007, ApJS, 171, 447
Robitaille, T. P., Whitney, B. A., Indebetouw, R., Wood, K., & Denzmore, P. 2006, ApJS, 167, 256
Sandell, G., & Weintraub, D. A. 2001, ApJS, 134, 115
Surace, J. A., et al. 2004, The SWIRE ELAIS N1 Image Atlases and Source Catalogs (Pasadena: *Spitzer* Science Center), http://ssc.spitzer.caltech.edu/legacy
Wainscoat, R. J., et al. 1992, ApJS, 83, 111
Walborn, N. R. 1972, AJ, 77, 312
Walker, M. F. 1959, ApJ, 130, 57
Ward-Thompson, D., et al. 2007, PASP, 119, 855
Young, K. E. 2005, ApJ, 628, 283
Zacharias, N., Monet, D. G., Levine, S. E., Urban, S. E., Gaume, R., & Wycoff, G. L. 2004, BAAS, 36, 1418